Multidecadal ozone trends in China and implications for human health and crop yields: A hybrid approach combining chemical transport model and machine learning

Jia Mao[1], Amos P. K. Tai[1,2,3], David H. Y. Yung[1], Tiangang Yuan[1], Kong T. Chau[1], and Zhaozhong Feng[2,4]

[1] Earth and Environmental Sciences Programme and Graduate Division of Earth and Atmospheric Sciences, Faculty of Science, The Chinese University of Hong Kong, Sha Tin, Hong Kong SAR, China

[2]Collaborative Innovation Center on Forecast and Evaluation of Meteorological Disasters (CIC-FEMD), Nanjing University of Information Science and Technology, Nanjing 210044, Jiangsu, China

[3] State Key Laboratory of Agrobiotechnology, and Institute of Environment, Energy and Sustainability, The Chinese University of Hong Kong, Hong Kong SAR, China

[4] Key Laboratory of Ecosystem Carbon Source and Sink, China Meteorological Administration (ECSS-CMA), Nanjing University of Information Science & Technology, Nanjing, 210044, China

Correspondence to: Amos P. K. Tai (amostai@cuhk.edu.hk)

Abstract. Surface ozone (O_3) is well known to pose significant threats to both human health and crop production worldwide. However, a multi-decadal assessment of O_3 impacts on public health and crop yields in China is lacking due to insufficient long-term continuous O_3 observations. In this study, we used a machine learning (ML) algorithm to correct the biases of O_3 concentrations simulated by the chemical transport model from 1981–2019 by integrating multi-source datasets. The ML-enabled bias correction offers improved performance in reproducing observed O_3 concentrations, and thus further improves our estimates of O_3 impacts on human health and crop yields. The warm-season increasing trend of O_3 in Beijing-Tianjin-Hebei and its surroundings (BTHs), Yangtze River Delta (YRD), Sichuan Basin (SCB) and Pearl River Delta (PRD) regions are 0 .32 μg m^{-3} yr^{-1}, 0.63 μg m^{-3} yr^{-1}, 0.84 μg m^{-3} yr^{-1}, and 0.81 μg m^{-3} yr^{-1} from 1981 to 2019, respectively. In more recent years, O_3 concentrations experience more fluctuations in the four major regions. Our results show that only BTHs have a perceptible increasing trend of 0.81 μg m^{-3} yr^{-1} during 2013–2019. Using AOT40-China exposure-yield response relationships, the estimated relative yield losses (RYLs) for wheat, rice, soybean and maize are 17.6%, 13.8%, 11.3% and 7.3% in 1981, and increases to 24.2%, 17.5%, 16.3% and 9.8% in 2019, with an increasing rate of +0.03% yr^{-1}, +0.04% yr^{-1}, +0.27% yr^{-1} and +0.13% yr^{-1}, respectively. The estimated annual all-cause premature deaths induced by O_3 increase from ~55,900 in 1981 to ~162,000 in 2019 with an increasing trend of ~2,980 deaths yr^{-1}. The annual premature deaths related to respiratory and cardiovascular disease are ~34,200 and ~40,300 in 1998, and ~26,500 and ~79,000 in 2019, having a rate of change of –546 and +1,770 deaths yr^{-1} during 1998–2019, respectively. Our study, for the first time, used ML to provide a robust dataset of O_3 concentrations over the past four decades in China, enabling a long-term evaluation of O_3-induced crop losses and health impacts. These findings are expected to fill the gap of the long-term O_3 trend and impact assessment in China.

1 Introduction

Surface ozone (O_3), an important secondary air pollutant, is mainly generated through photochemical reaction of volatile organic compounds (VOCs), carbon monoxide (CO), and nitrogen oxides (NO_x) in the presence of sunlight. As a strong oxidant, O_3 at the ground level is detrimental to human health and vegetation. More recently, due to the rapid urbanization and industrialization, the summertime O_3 pollution has become an emerging concern in China. Li et al. (2020) reported that the mean summer 2013–2019 trend in maximum daily 8-h average surface O_3 (MDA8-O_3) was +1.9 ppb yr^{-1} in China, with high values widely observed in the North China Plain (NCP), Yangtze River Delta (YRD), and Pearl River Delta (PRD) regions. On the regional scale, the exposure of humans and vegetation to O_3 is greater in China than in other developed regions of the world (Lu et al., 2018). Several studies have suggested the important roles of climate and land cover changes on O_3 pollution in addition to anthropogenic emissions (Fu and Tai, 2015; Wang et al., 2020). It has been suggested that global warming and the changing land use may further increase surface O_3 by the late 21st century (Kawase et al., 2011; Wang et al., 2020), which can pose greater threats to human health and food security.

Meteorological factors can modulate the temporal and spatial patterns of O_3 via affecting the physical and chemical processes within the atmosphere (Liu et al., 2019; Mao et al., 2020; Yin and Ma, 2020). High temperature, low relative humidity and low planetary boundary height are conducive to the photochemical production and O_3 accumulation. Jacob and Winner (2009) summarized that the enhanced O_3 levels at higher temperatures are primarily driven by increased biogenic VOC emissions from vegetation and reduced lifetimes of peroxyacetyl nitrate (PAN) due to accelerated decomposition of PAN into NO_x. Besides, the changes in wind speed and direction can affect O_3 concentrations through transport. Land cover and land use change affects O_3 air quality by perturbing surface fluxes, hydrometeorology, and concentrations of atmospheric chemical components (Tai et al., 2013; Fu and Tai, 2015; Liu et al., 2020; Ma et al., 2021). For instance, the terrestrial biosphere is a major source of isoprene, which plays a significant role in modulating O_3 concentrations. In the Intergovernmental Panel on Climate Change (IPCC) A1B scenario, Tai et al. (2013) found that widespread crop expansion could reduce isoprene emission by ~10 % globally compared with the present land use. Such a reduction could decrease O_3 by up to 4 ppb in the eastern US and increase O_3 by up to 6 ppb in South and Southeast Asia, whereby the difference in the sign of responses is primarily determined by the different O_3 production regimes.

The increasing health burden due to air pollution has become an important contributor to global disease burden. Some recent studies have demonstrated that short-term O_3 exposure negatively impacts human health, especially via respiratory, and cardiovascular mortality (Shang et al., 2013; Yin et al., 2017b; Feng et al., 2019; Zhang et al., 2022a). In 2015–2018, the estimated annual total premature mortality related to O_3 pollution in 334 Chinese cities was 0.27 million for 2015, 0.28 million for 2016, 0.39 million for 2017, and 0.32 million for 2018 (Zhang et al., 2021). Maji and Namdeo (2021) reported that short-term all-cause, cardiovascular and respiratory premature mortalities attributed to the ambient 4th highest MDA8-O_3 exposure were 156,000, 73,500 and 28,600 in 2019, showing increases of 19.6%, 19.8% and 21.2%, respectively, compared to 2015. Zhang et al. (2022b) reported that each 10 μg m^{-3} increase in the MDA8-O_3 can lead to a rise of 0.41 % (95 % CI: 0.35 %–0.48 %) in all-cause, 0.60 % (95 % CI: 0.51 %– 0.68 %) in cardiovascular and 0.45 % (95 % CI: 0.28 %– 0.62 %) in respiratory mortality.

The damage to plants induced by O_3 is mainly caused by the stomatal uptake of O_3 into the leaf interior instead of direct plant surface deposition (e.g., Clifton et al., 2020). In previous studies, a variety of concentration-based metrics have been widely used to assess the O_3 risks to crop yield and ecosystem functions. Initially, a 7-hour (09:00–15:59) mean metric (M7) was proposed, which was later extended to a 12-hour (08:00–19:59; referred to M12) to include late-day O_3 concentrations. Cumulative metrics have also been developed to evaluate the impacts of O_3 on crops. The accumulated O_3 over a threshold of 40 ppb (AOT40) is a widely used metric to evaluate the phytotoxic effects of O_3. Compared to AOT40 using a linear function, another metrics, W126, considers the nonlinear response of yield loss to O_3 exposure whereby higher O_3 concentrations will progressively induce more severe yield losses. However, many studies have suggested that the stomatal uptake of O_3 is more related to vegetation damage than O_3 exposure per se (Feng et al., 2012; Feng et al., 2018; Pleijel et al., 2022). In the recent two decades, the flux-based approach therefore has been developed and increasingly used to assess the relationships between the stomatal O_3 uptake and crop yields. Tai et al. (2021) compared the results of the estimated global crop yield losses using three concentration-based and two flux-based O_3 exposure metrics, and showed that the concentration-based metrics differ greatly among themselves, while the two flux-based metrics are generally close to each other, which lie close to the middle of the range covered by all metrics.

At present, a comprehensive long-term assessment of O_3 impacts is hindered by a lack of continuous O_3 observations in China (Lu et al., 2018; Gong et al., 2021). From both health and food perspectives, reliable long-term estimates of O_3 are critically needed to better understand the O_3 damage over the past few decades since the beginning of rapid industrial transformation in the 1980s. In previous studies, various alternative approaches have been used to address the problem of insufficient observations. The multiple linear regression (MLR) model is often used for extrapolation to construct spatiotemporal distributions of air pollutants (Moustris et al., 2012; Abdullah et al., 2017). However, the linear statistical methods are generally limited by their incapability to capture the nonlinear relationships between air pollutants and precursors as well as meteorological fields. Chemical transport models (CTMs), based on mathematical representation of atmospheric physical and chemical processes, are also the common tool to simulate air pollutant concentrations spatiotemporally (Fusco and Logan, 2003; Liu and Wang, 2020a; Wang et al., 2022a). Taking the advantages of the CTM, Fu and Tai (2015) investigated the impacts of historical climate and land cover changes on tropospheric O_3 in East Asia between 1980 and 2010. However, the utility of CTMs is often limited by their high computational cost when conducting long-term simulations at high spatiotemporal resolutions. Large biases also exist due to uncertainties in historical emission inventories, parameterization of physical and chemical processes, and initial and/or boundary conditions, and these errors tend to increase at finer spatiotemporal scales.

In recent years, machine learning (ML) methods have gained increasing popularity in air pollution studies (Liu et al., 2020; Ma et al., 2021). In the early stage of applying ML to atmospheric chemistry, ML methods were usually used as an independent method from CTMs (Hu et al., 2017; Zhan et al., 2017), for instance, to predict O_3 concentrations by mapping the nonlinear relationships between observed O_3 concentrations and their possible shaping factors. These applications are usually purely data-driven, whereby the ML algorithms do not involve any representation of the physical mechanisms behind the relevant processes. With powerful algorithms and user-friendly hyperparameter tuning processes, some well-trained ML models, driven by data from multiple sources including reanalysis and satellite data, have shown even higher predictive capacity than process-based models. The advantages of ML methods over CTMs include more flexible choices for input data and spatiotemporal resolution, and substantially lower computational costs (Bi et al., 2022). However, purely data-driven ML methods are known to suffer a lack of transparency and interpretability, which renders it more difficult to offer adequate scientific interpretation for the physical mechanisms behind. Thus, a hybrid approach combining ML algorithms and CTM-simulated results have been increasingly used to predict air pollutants and understand their trends in recent years. Integrating data from various sources, ML methods have been used as a tool to correct the biases in the lower-resolution simulated results from CTMs (Di et al., 2017; Ivatt and Evans, 2020; Ma et al., 2021). Based on process-based CTMs integrating decades of accumulated knowledge in Earth system science, while taking advantage of ML to address still-existing model errors, the hybrid approach has great potential in tackling air quality problems (Irrgang et al., 2021).

In this work, we incorporated the O_3 concentrations directly simulated by the Goddard Earth Observing System coupled with Chemistry (GEOS-Chem) model at a lower resolution into a bias-corrected, finer-resolution dataset by integrating them with O_3 observations from 2016 to 2018 (for validation purpose), high-resolution metetrological fields, land use data and other geographical information from multiple sources using a tree-based ML algorithm, LightGBM. The final high-resolution hourly O_3 dataset with a resolution of 0.25°×0.25° from 1981 to 2019 was further used to assess the impacts of O_3 on human health and crop yields over the past four decades. The simultaneous analysis of the combined impacts of O_3 on agriculture and human health can offer more comprehensive policy implications for the mitigation of O_3-related impacts across China.

2 Data and methods

2.1 Air quality, meteorological, land and crop data

Hourly surface O_3 observations (μg m^{-3}) from 2016 to 2018 were obtained from the China National Environment Monitoring Center Network (http://106.37.208.233:20035/) established by the Ministry of Ecology and Environment of China. The MDA8-O_3 of each site was calculated with at least 14 valid hourly values from 08:00 to 24:00 local time. A total of 1016 sites were selected after deleting the missing and abnormal data (**Fig. 1**).

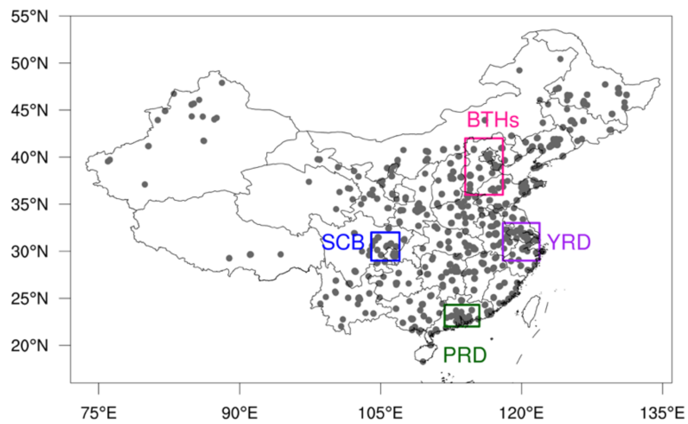

Figure 1. Study domain and locations of the selected monitoring sites. The pink, blue, purple and green rectangles indicate the Beijing-Tianjin-Hebei and its surroundings (BTHs), Sichuan Basin (SCB), Yangtze River Delta (YRD), and Pearl River Delta (PRD) regions, respectively, for more detailed analysis.

The surface meteorological fields used in this study include sea surface pressure, horizontal wind at 10 m, air temperature at 2 m, downward solar radiation, surface albedo, and total precipitation. The variables selected at 850 hPa and 100 hPa include relative humidity, horizontal and vertical velocity. These meteorological variables have been shown by many previous studies to correlate strongly with surface O_3 concentrations as discussed above. Hourly reanalysis data for meteorological variables were obtained from the fifth generation European Center for Medium-Range Weather Forecasts (ECMWF) reanalysis dataset (ERA5) with a spatial resolution of 0.25°×0.25° from 1981 to 2019 (https://cds.climate.copernicus.eu/). This spatial resolution sets the highest limit of resolution for our hybrid O_3 product.

The national land use data with a spatial resolution of 1 km×1 km for 2013 were obtained from the Resource and Environment Science Data Center of the Chinese Academy of Sciences (RESDC) (http://www.resdc.cn). Six primary types of land use are considered: cultivated land, forestland, grassland, water bodies, construction land, and unused land. Nationwide elevation data were also provided by the RESDC (https://www.resdc.cn/data.aspx?DATAID=123), which is resampled based on the latest Shuttle Radar Topography Mission (SRTM) V4.1 data developed in 2000.

The spatial distribution of the harvested areas for four staple crops (wheat, rice, maize, soybean) for China was obtained from the Global Agro-Ecological Zones 2015 dataset (https://doi.org/10.7910/DVN/KJFUO1). Crop harvesting dates with a resolution of 0.5°×0.5° were provided by the Center for Sustainability and the Global Environment (Sacks et al., 2010). For crops having more than one growing season in a year, only the primary growing period was considered.

2.2 GEOS-Chem model

We used the GEOS-Chem global 3-D chemical transport model version 12.2.0 (http://acmg.seas.harvard.edu/geos/), driven by assimilated meteorological data from Modern Era Retrospective-analysis for Research and Applications, Version 2 (MERRA2) (https://gmao.gsfc.nasa.gov/reanalysis/MERRA-2/) with a horizontal resolution of 2.0° latitude by 2.5°

longitude and reduced vertical resolution of 47 levels. GEOS-Chem incorporates meteorological conditions, emissions, chemical information, and surface conditions to simulate the formation, transport, mixing and deposition of ambient O_3. It performs fully coupled simulations of O_3-NO_x-VOC-aerosol chemistry (Bey et al., 2001). Previous studies have demonstrated the ability of GEOS-Chem to reasonably reproduce the magnitudes and seasonal variations of surface O_3 East Asia (Wang et al., 2011; He et al., 2012). To provide long-term simulated O_3 fields for incorporation into the ML model (see below), we conducted GEOS-Chem simulations at a resolution of 2.0°×2.5°; higher resolutions of GEOS-Chem in nested grids are available but computationally prohibitive for multi-decadal simulations. The original unit of GEOS-Chem-simulated O_3 is ppb, which was converted to μg m^{-3} assuming a constant temperature of 25°C and pressure of 1013.25 hPa (1 μg m^{-3} is approximately 0.5 ppb) when compared with observations (Yin et al., 2017b; Gong and Liao, 2019).

Global anthropogenic emissions of CO, NO_x, SO_2 and VOCs are from Community Emissions Data System (CEDS), which has coverage over the simulation years of 1950–2014 (Hoesly et al., 2018). Biomass burning emissions are from the GFED-4 inventory (van der Werf et al., 2017). Biogenic VOC emissions are computed by the Model of Emissions of Gases and Aerosols from Nature (MEGAN) v2.1 (Guenther et al., 2012), which is embedded in GEOS-Chem. Emissions of biogenic VOC species in each grid cell, including isoprene, monoterpenes, methyl butenol, sesquiterpenes, acetone and various alkenes, are simulated as a function of canopy-scale emission factors modulated by environmental activity factors to account for changing temperature, light, leaf age, leaf area index (LAI), soil moisture and CO_2 concentrations (Sindelarova et al., 2014).

Dry deposition follows the resistance-in-series scheme of Wesely (1989), which depends on species properties, land cover types and meteorological conditions, and uses the Olson land cover classes with 76 land types reclassified into 11 land types. Although transpiration is a potential mechanism via which the land cover affects ozone, we do not address it in this study because water vapor concentration in GEOS-Chem is prescribed from assimilated relative humidity (i.e., not computed online from evapotranspiration).

2.3 LightGBM machine-learning model

In this study, we used the LightGBM algorithm to integrate GEOS-Chem simulated O_3 at a lower resolution with higher-resolution multi-source data to produce higher-resolution hourly O_3 and MDA8-O_3 fields. Because the representation of input data for LightGBM should be regular, datasets at different spatial resolutions were all regridded to a unified resolution of 0.25°×0.25° with the operationally used bilinear interpolation approach (e.g., Accadia et al., 2003), consistent with the meteorological fields. By taking the advantage of these high-resolution datasets, the hybrid approach can not only correct the biases of the GEOS-Chem-simulated O_3, but also refine it into a finer resolution. LightGBM is a ML algorithm based on the gradient boosting decision tree (Chen and Guestrin, 2016), which has a high training efficiency and lower memory footprint, and thus is suitable for processing massive high-dimensional data (Zhang et al., 2019). The general steps to build a ML model can be summarized as follows: (1) choose an algorithm appropriate for the problem (e.g., regression or classification); (2) clean the data and split them into training and test data; (3) train and tune the model with training data to well capture prediction patterns; (4) evaluate model performance on test data; and (5) return to step (3) and (4) until an optimal predictive ability is reached. The whole dataset is divided into training and test data to evaluate the model generalization ability. The model performance on test data can indicate whether the model can perform well on new data independent of the training process.

During the model training process, the model was evaluated with 10-fold cross-validation to ensure the robustness and reliability of the model, whereby the training data were randomly partitioned into 10 subsets of approximately the same size, with 90% of data used to train individual models and the ensemble model, and the remaining 10% of data used to examine model performance (Xiao et al., 2018). This process was repeated 10 times so that each data record was left for testing once. The tuning of the hyperparameters was optimized using grid search optimization to improve detection performance and diagnostic accuracy (Wang et al., 2019). Statistical indicators, including the coefficient of determination (R^2) and root-mean-square error (RMSE), were used in subsequent assessment of model performance for GEOS-Chem alone and for the hybrid approach. During evaluation, the model results in the grid cell covering or closest to each site were utilized to compare with observations. This approach of comparing model simulated gridded air pollutant concentrations (either from a CTM or ML model) against site-level observations has been commonly used to evaluate model performance (Ma et al., 2021; Meng et al., 2022; Thongthammachart et al., 2021). Additionally, when comparing the GEOS-Chem-simulated O_3 with observations, the simulated O_3 was first regridded to 0.25°×0.25° using the operationally used bilinear interpolation approach to maintain consistency with the ERA5 dataset.

Our analysis revealed that training the model with one year or more of data results in only marginal reductions in RMSE and enhancements in R^2 (**Fig. S1**); thus a timescale of two years appears to strike a good balance between computational burden and model accuracy. These results align with the findings of Ivatt and Evans (2020), who suggested that much of the variability in the power spectrum of surface O_3 can be captured by timescales of a year or less. Therefore, here we utilized observations from the period 2016-2017 as the training data, which offered a more economical computing cost and improved training time efficiency, and observations in 2018 as the independent test data to evaluate model performance.

2.4 Ozone exposure metric and exposure–yield response functions

Among O_3 exposure indices, AOT40 has been used widely during the last two decades as it has been found to have a strong relationship with relative yield of many crop species (Mills et al., 2007), and thus was used to quantify the impacts of surface O_3 on crop yields in this study. The flux-based metrics, which require long-term simulations using a process-based stomatal uptake model, were beyond the scope of this study. The AOT40 (ppm-h) is defined as follows:

$$\mathrm{AOT40} = \sum_{i=1}^{n}([\mathrm{O_3}]_i - 0.04) \tag{1}$$

where the $[O_3]_i$ is the hourly mean O_3 concentration (ppm) during the 12 hours of local daytime (08:00–19:59); n is the number of hours in the growing season defined as the 90 days prior to the start of the harvesting period according to the crop calendar.

The exposure–yield response functions based on extensive field experimental studies have been established to relate a quantifiable O_3-exposure metrics to crop yields. It has been suggested that responses of crop yields were found greater in Asian experiments than the American and European counterparts, indicating possibly higher O_3 sensitivity of Asian crop varieties (Emberson et al., 2009; Feng et al., 2022).To better understand O_3-induced risks to crops in China, the AOT40 exposure-yield functions developed based on field experiments in China are used in this study, which are named as AOT40-China. The exposure–yield response functions for soybean is from Zhang et al. (2017), and for other three crops are from Feng et al. (2022). The statistical exposure-yield relationships used in this study are summarized in **Table S1**.

2.5 Analysis of health impacts

All-cause mortality, cardiovascular disease mortality and respiratory disease mortality are selected as the health outcomes of our study due to the high correlation between these endpoints and short-term O_3 exposure in previous studies. A log-linear exposure-response function is widely adopted and recommended by the World Health Organization (WHO) for health impact assessment in areas with severe air pollution. In particular, the log-linear model is the most widely applied exposure-response model at present in China (Lelieveld et al., 2015; Yin et al., 2017a; Zhang et al., 2022b). The premature mortality is calculated following:

$$\Delta M = \delta c * \left[\frac{(\mathrm{RR}-1)}{\mathrm{RR}}\right] * P \quad (2)$$

where ΔM is the excess mortality attributable to O_3 exposure; δc is the baseline mortality rate for a particular health endpoint (Yin et al., 2017b; Madaniyazi et al., 2016); P is the exposed population; and RR is the relative risk defined as:

$$\mathrm{RR} = \exp(\,(X - X_0) * \beta) \quad (3)$$

where β is the exposure-response coefficient derived from epidemiological cohort studies (Shang et al., 2013); X represents the model-calculated O_3 concentration; the value of X_0 is the threshold concentration below which no additional risk is assumed. Consistent with previous studies (Lelieveld et al., 2015; Liu et al., 2018), we used $X_0 = 75.2$ µg m^{-3}.

In this study, the mean MDA8-O_3 concentrations in warm season (May-September) were used to estimate the disease-specific health impacts of short-term exposure to O_3. The province-level population and national baseline mortality rate for particular diseases were provided by the National Bureau of Statistics (http://www.stats.gov.cn/). The spatial differences of baseline mortality in China were not considered without provincial-level data, which means that we assume the baseline mortality is evenly distributed across China (Dedoussi et al., 2020). The exposure-response coefficients were obtained from existing epidemiological studies in China (**Table S2**). If the corresponding coefficient of a province could not be found in published epidemiological studies, the datum closest to that province would be selected as a substitute. If there were no neighboring provinces, the results of national meta-analysis would be used (Zhang et al., 2021).

3 Results

3.1 Model development and validation

The finally selected features and their importance estimated by the LightGBM algorithm based on 10-fold cross validation are shown in **Fig. 2**. GEOS-Chem-simulated O_3 is the top predictor for predicting surface O_3 concentrations, accounting for 61% and 58% of all relative importance in the ML algorithm predicting hourly O_3 and daily MD8A-O_3, respectively. The result indicates that process-based GEOS-Chem simulations have high utility for O_3 predictions under the hybrid approach (Ma et al., 2021). The meteorological variables with high contribution to both the daily and hourly models are downward surface solar radiation (SSRD), relative humidity at 1000 hpa (RH_1000hpa) and 10-m horizontal wind (U10 and V10). Other special features, including location (latitude and longitude), elevation and diurnal and monthly pattern of O_3, also contribute to ambient O_3 estimations. The spatial distributions of bias-corrected O_3 are consistent with observations for both training and test datasets (**Fig. S2**), indicating that there is no obvious overfitting, i.e., the model is able to generalize from the training set to the test set. The good generalization ability of the model gives us confidence in its ability to make accurate predictions based on new data. In general, the hybrid approach can yield good O_3 estimates in the data-intensive regions, including eastern and central China that are the hotspot areas of O_3 pollution.

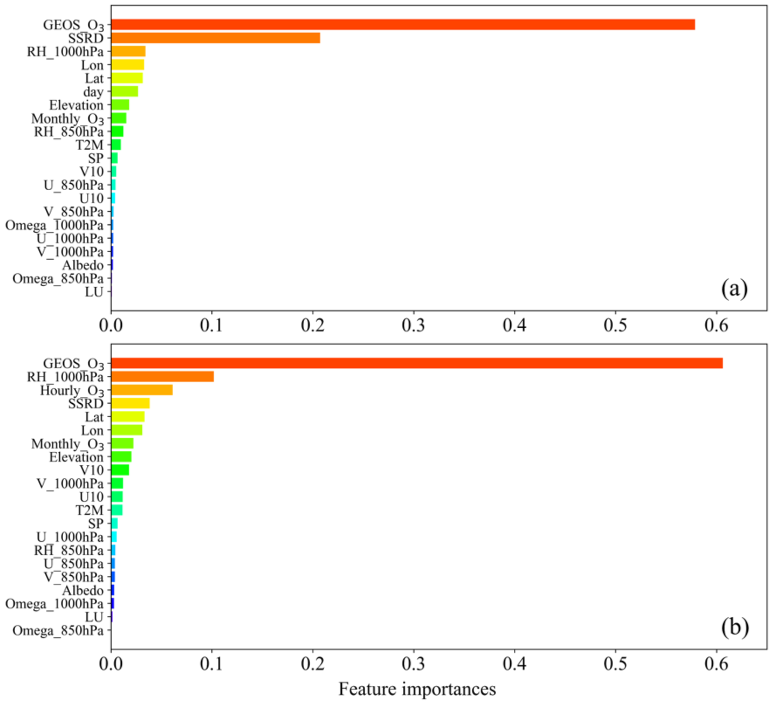

Figure 2. The feature importance plot for (a) MDA8-O_3 and (b) hourly O_3, respectively. The full list of candidate variables with their symbols, units, descriptions, and data sources are shown in Table S3.

Fig. 3 shows the density scatter plots between O_3 measurements and GEOS-Chem simulations, as well as the hybrid-approach predictions for 2018. The R^2 value of the hybrid approach and GEOS-Chem model are 0.66 and 0.27 at hourly level, and 0.72 and 0.53 at MDA8-O_3 level, respectively. Bias-corrected O_3 concentrations have lower RMSE in comparison with GEOS-Chem simulated O_3 concentrations, reduced from 31.1 to 23.8 μg m^{-3} for MDA8-O_3 predictions, and from 38.5 to 26.3 μg m^{-3} for hourly predictions. The MDA8-O_3 model performance is better than that of the hourly model, indicating reduced errors upon temporal averaging. The MERRA2 dataset driving GEOS-Chem was also used to train the model; however, we found that the higher-resolution ERA5 dataset performed better in reproducing observed O_3 concentrations with smaller RMSE and larger R^2 (**Fig. S3**). This analysis demonstrates the level to which a higher-resolution meteorological dataset, despite not being strictly consistent with the input meteorology for the CTM, can help enhance the performance of the hybrid model. In summary, the result suggests that the CTM-simulated results can be substantially improved by applying ML with multi-source datasets, and the bias-corrected data can improve our understanding of long-term O_3 trends and its further implications on crop and human health over China, as discussed in the following sections.

In comparison with previous studies, Liu et al. (2020) used XGBoost to predict O_3 in major urban areas of China at a resolution of 0.1°×0.1°, and the R^2 value and RMSE for MDA8-O_3 were 0.74 and 23.8 μg m^{-3}, respectively. Their result indicates that higher-resolution predictions may help enhance model accuracy, but represent a trade-off between model accuracy and time efficiency depending on the purpose. Instead of directly predicting O_3 concentrations, Ivatt and Evans (2020) predicted biases in GEOS-Chem-simulated O_3 concentrations and then corrected them with XGBoost. They also suggested that the corrected model performs considerably better than the uncorrected model, with RMSE reduced from 32.4 to 15.0 μg m^{-3} and Pearson's R raised from 0.48 to 0.84. Their greater improvement with larger reduced RMSE than our result is mainly because they selected fewer sites for training, with all the urban and mountain sites (observations made at a pressure < 850 hPa) removed. The removal of these sites can improve the overall apparent performance of the model because O_3 formation could have different characteristics in these areas. In general, ML methods have been proven to be a promising tool to improve air pollutant forecasts when a process-level understanding is still incomplete.

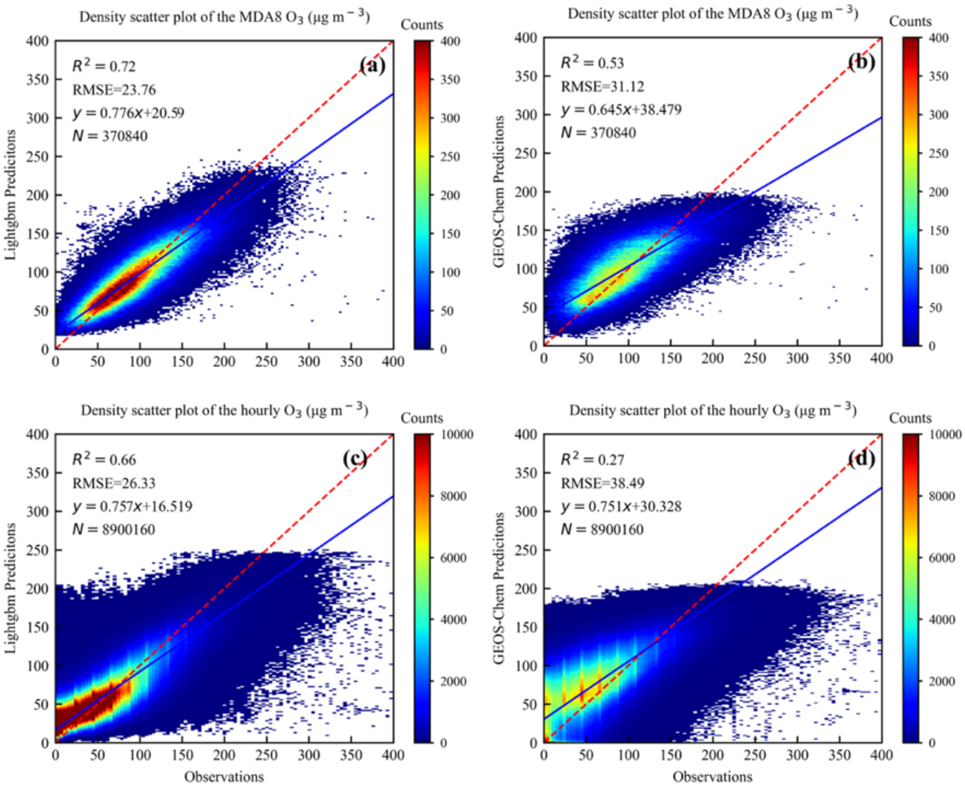

Figure 3. Density scatter plots and linear regression statistics of O_3 predictions vs. observation for 2018: (a) bias-corrected MDA8-O_3 vs. observations; (b) GEOS-Chem MDA8-O_3 vs. observations; (c) bias-corrected hourly O_3 vs. observations; and (d) GEOS-Chem hourly O_3 vs. observations. The dashed red line indicates the 1:1 line, and the solid blue line indicates the line of best fit using orthogonal regression. The R^2 is the coefficient of determination, RMSE is the root-mean-square error, and N is the number of data points. The X and Y axis represents the O_3 observations and predictions, respectively.

3.2 Spatiotemporal distribution and trends of O_3 predictions

Fig. 4 demonstrates the spatial patterns of averaged annual and warm-season (May-September) MDA8-O_3 from 1981 to 2019. When compared to the high concentrations in the warm season, MDA8-O_3 concentrations are relatively lower at annual level. The annual and warm-season MDA8-O_3 concentrations have similar spatial distribution, and both present an increasing trend over the past decades, with more substantial increase observed between 1981 and 2010. The O_3 levels in southern China are lower than those in northern China, but they are still relatively high in the PRD region, which is consistent to findings in previous studies (e.g. Liu and Wang, 2020a). During the first decade of 1981–1990, high O_3 concentration areas are mainly concentrated in the BTHs and northern Shandong. In the next two decades, O_3 pollution extensively expands to most of East and North China, spreading northward to Jilin and Liaoning, westward to Shanxi and Ningxia, and southward to northern Hunan, Shanxi and Zhejiang. Moreover, the SCB and PRD regions also experience aggravated O_3 pollution during this period. In the last decade of the study period, O_3 concentrations remain at high levels in BTHs and SCB without obvious changes. To understand the detailed changes and trends of O_3, next we analyze the interannual variability.

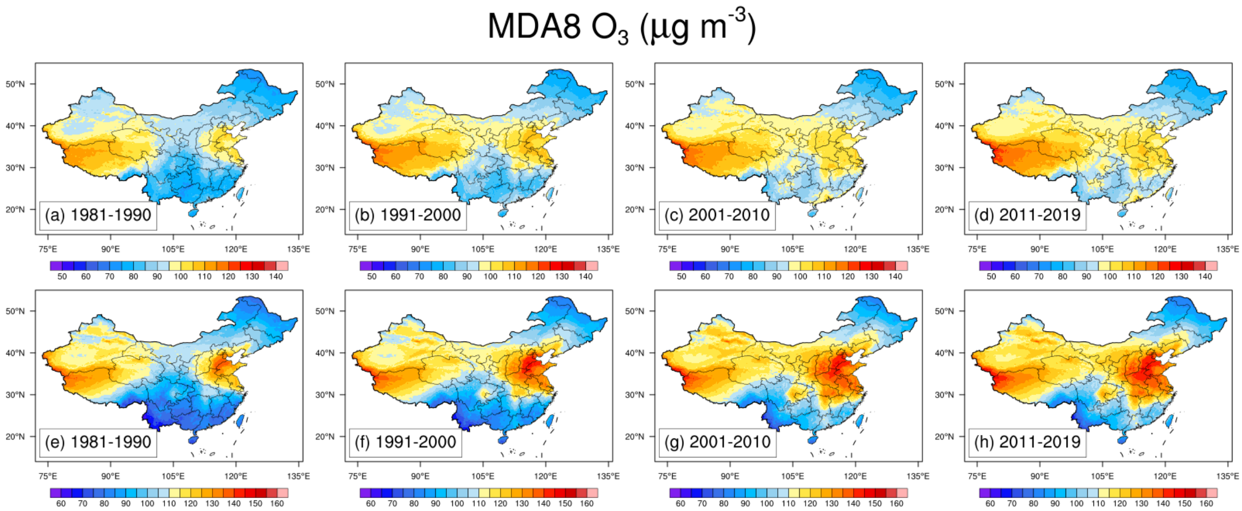

Figure 4. Spatial distribution of the annual mean MDA8-O_3 concentrations (μg m^{-3}) during: (a) 1981–1990; (b) 1991–2000; (c) 2001–2010; and (d) 2011–2019. Spatial distribution of the warm-season (May-September) mean MDA8-O_3 concentrations of (e)1981–1990, (f) 1991–2000, (g) 2001–2010; and (h) 2011–2019.

Fig. 5 shows that the annual averaged MDA8-O_3 concentrations increase from 87 μg m^{-3} in 1981 to 98 μg m^{-3} in 2019, with a growth rate of +0.26 μg m^{-3} yr^{-1}, while the warm-season averaged MDA8-O_3 concentrations increase from 100 μg m^{-3} in 1981 to 117 μg m^{-3} in 2019, having a growth rate of +0.51 μg m^{-3} yr^{-1}. Moreover, the average annual and warm-season O_3 concentrations have a more obvious upward trend before 2000s, with a growth rate of 0.38 μg m^{-3} yr^{-1} and 0.71 μg m^{-3} yr^{-1}, compared to that after 2000s, when O_3 concentrations appear to fluctuate within a certain range. GEOS-Chem-simulated O_3 has a similar trend as the bias-corrected O_3, but it generally overestimates O_3 concentrations on national scale (**Fig. S4**). The annual and warm-season averaged MDA8-O_3 concentrations in BTHs, YRD, SCB and PRD regions are shown in **Fig. S5–S6**. The warm-season increasing trend for BTHs, YRD, SCB and PRD regions are 0.32 μg m^{-3} yr^{-1}, 0.63 μg m^{-3} yr^{-1}, 0.84 μg m^{-3} yr^{-1}, and 0.81 μg m^{-3} yr^{-1} from the year 1981 to 2019.

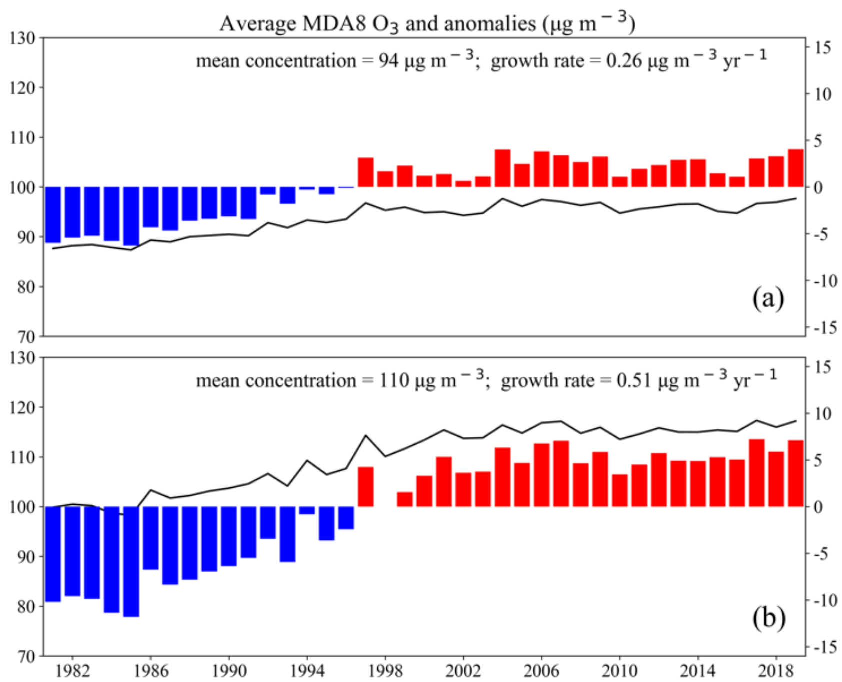

Figure 5. The bias-corrected MDA8-O_3 predictions (black line; left y axis) and corresponding anomalies (colored

bar; right y axis) from 1981 to 2019: (a) annual mean; and (b) warm-season mean (May-September). The trends (growth rates) are obtained by ordinary linear regression on mean values of MDA8-O_3. The anomalies are defined as annual mean minus the multidecadal average over 1981–2019.

In recent years, the worsening O_3 pollution has fueled numerous studies on ground-level O_3 spatial distribution and changes in China, which were conducted on local, regional and national scale using different O_3 fields from observations, CTMs and ML estimates. In this study, we mainly focus on the regional and national O_3 characteristics, and the reported O_3 trends in recent studies are listed in **Table 1**. By comparing the results of existing works, we find that source-varied O_3 fields can induce great uncertainty of the O_3 trends. Moreover, the O_3 trends are found to be very sensitive to the study period even with the same O_3 fields (Wei et al., 2022), which indicates large interannual variability, mostly reflecting the changing anthropogenic emissions and meteorology (Lu et al., 2019; Li et al., 2020). In contrast to the perceptible O_3 trends, Liu et al. (2020) suggested that O_3 pollution in most parts of China has only modest changes between 2005 and 2017, and their trends were not spatially continuous. Wang et al. (2022b) also reported that O_3 has small positive increase rates for 2013–2021 in many cities, and the O_3 increase rates greatly differ from site to site even within the same region.

In comparison, our results indicate no obvious increasing trends of national MDA8-O_3 within the same study period. On a regional scale, only BTHs have a perceptible increasing trend in more recent years, while no such trends are found over the YRD, SCB and PRD regions during the same period. The summertime MDA8-O_3 in BTHs has a change rate of +0.81 $\mu g\ m^{-3}\ yr^{-1}$, which is much lower than the results using O_3 observations (Li et al., 2020). One possible reason is that most observational sites are in urban regions, which usually suffer more serious O_3 pollution, while the O_3 concentrations from model simulations and ML methods are calculated on the scale of a grid cell with lower domain-averaged values. Moreover, gridded data at a relatively coarse resolution may fail to capture larger site differences, leading to the larger discrepancy of between O_3 observations and gridded O_3 estimates.

Table 1 Summary of reported regional and national MDA8-O_3 trends ($\mu g\ m^{-3}\ yr^{-1}$).

Region	Period	Increase rate	Data source/Method	References
Nation	2013–2017 (annual)	0.35	ML (XGBoost)	(Liu et al., 2020)
	2013–2017 (annual)	0.92	WRF-CMAQ	(Liu and Wang, 2020b)
	2013–2017 (annual)	1.33	ML (ERT)	(Wei et al., 2022)
	2015–2019 (annual)	4.40	ML (ERT)	(Wei et al., 2022)
	2015–2019 (annual)	1.90	Observations	(Maji and Namdeo, 2021)
	2013–2019 (summer)	3.80	Observations	(Li et al., 2020)
	1981–2019 (annual)	0.26	ML (LightGBM)	This study
	1981–2000 (annual)	0.38	ML (LightGBM)	This study
	1981–2019 (warm-season)	0.51	ML (LightGBM)	This study
	1981–2000 (warm-season)	0.71	ML (LightGBM)	This study
BTH	2010–2017 (annual)	0.60	ML (Random Forest)	(Ma et al., 2021)
	2013–2017 (annual)	1.33	ML (XGBoost)	(Liu et al., 2020)
	2013–2017 (annual)	4.78	ML (ERT)	(Wei et al., 2022)
	2012–2017 (summer)	1.16	GEOS-Chem	(Dang et al., 2021)
	2013–2019 (summer)	6.60	Observations	(Li et al., 2020)
	1981–2019 (summer)	0.46	ML (LightGBM)	This study
	2013–2019 (summer)	0.81	ML (LightGBM)	This study
YRD	2013–2017 (annual)	2.94	ML (ERT)	(Wei et al., 2022)
	2015–2019 (annual)	5.60	ML (ERT)	(Wei et al., 2022)
	2012–2017 (summer)	3.48	GEOS-Chem	(Dang et al., 2021)
	2013–2019 (summer)	3.20	Observations	(Li et al., 2020)
	1981–2019 (annual)	0.24	ML (LightGBM)	This study
	1981–2019 (summer)	0.73	ML (LightGBM)	This study
SCB	2013–2017 (annual)	2.37	ML (ERT)	(Wei et al., 2022)

	2013–2019 (summer)	1.40	Observations	(Li et al., 2020)
	1981–2019 (annual)	0.48	ML (LightGBM)	This study
	1981–2019 (summer)	0.98	ML (LightGBM)	This study
PRD	2007–2017 (annual)	1.20	Observations	(Yang et al., 2019)
	2013–2017 (annual)	–0.72	ML (ERT)	(Wei et al., 2022)
	2015–2019 (annual)	4.38	ML (ERT)	(Wei et al., 2022)
	2013–2019 (summer)	2.20	Observations	(Li et al., 2020)
	1981–2019 (annual)	0.56	ML (LightGBM)	This study
	1981–2019 (fall)	0.69	ML (LightGBM)	This study

3.3 Seasonal characteristics of O_3 predictions

Differences in averaged annual and warm-season O_3 concentrations indicate that O_3 has distinctive seasonal characteristics. **Fig. 6** shows the seasonal variations in O_3 concentrations from 2011–2019, and results for other past three decades are shown in **Fig. S7-S9**. In winter, pollution is mainly concentrated in the coastal areas of southern China. In spring, O_3 pollution primarily occurs in eastern China and the southern part of Yunnan Province. O_3 pollution continues to aggravate over eastern China in summer, particularly in BTHs, and further extends to SCB. The air quality in eastern and central China is greatly improved in fall, while southern China experiences the most pollution in this period. In general, the peak and trough values of O_3 concentrations appear in summer and winter, respectively. However, O_3 concentrations are found to be minimum in summer and maximum in fall over PRD, which is largely determined by the summer monsoon (Zhou et al., 2013; Wang et al., 2018a). **Fig. S10** shows the seasonal averaged MDA8-O_3 concentrations in different regions from 1981 to 2019. In winter, O_3 concentrations do not have much change across the four regions over the past decades, staying mostly between 70–80 μg m^{-3}. Moreover, wintertime O_3 concentrations after the 2000s are generally lower than that before the 2000s in BTHs, YRD and SCB. In contrast, summertime O_3 concentrations have a dramatic increase over the four regions. In spring and fall, O_3 concentrations have an increasing trend in PRD, while it mostly fluctuates within a certain range in the other three regions. The results show that O_3 in non-winter seasons has a more pronounced increase during 1981–2019 albeit with regional differences. The regional characteristics of O_3 and its influencing factors will be further discussed in Section 3.4. The BTH, SCB, YRD, and PRD regions have been identified as hotspots of O_3 pollution in China. These regions are characterized by high population density (Wang et al., 2018b) and are also major agricultural areas (Monfreda et al., 2008), which may face greater burdens of crop yield and human health losses with high O_3 concentrations. Therefore, here we provide more detailed analysis and investigation of these regions.

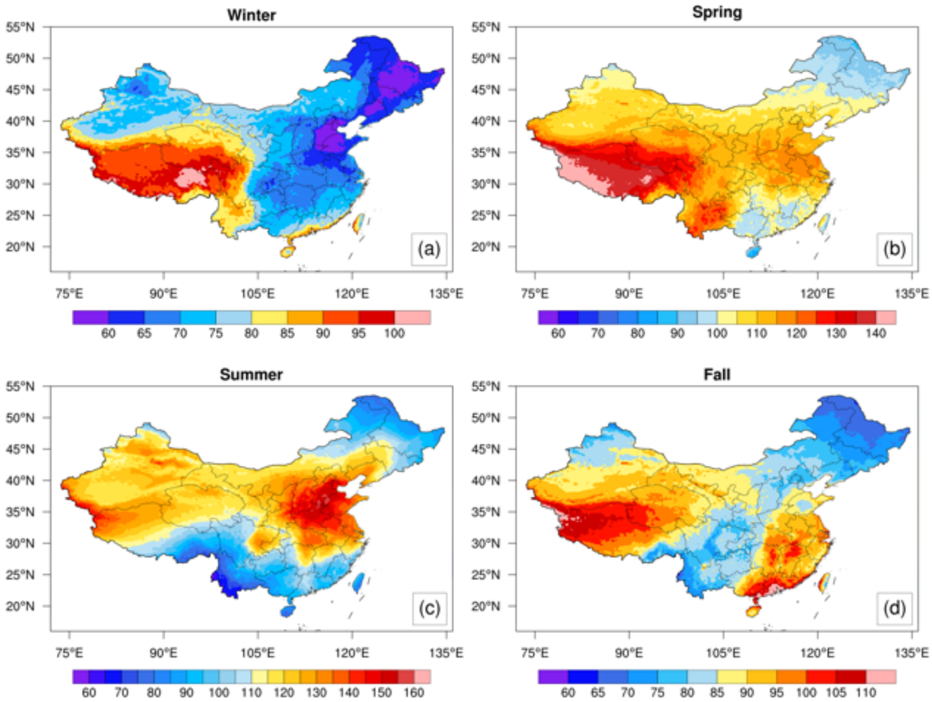

Figure 6. Spatial distribution of the bias-corrected MDA8-O_3 predictions ($\mu g\ m^{-3}$) from 2011–2019: (a) winter; (b) spring; (c) summer; and (d) fall.

3.4 Regional characteristics of O_3 predictions

Fig. 7 shows the bar plots of the seasonal MDA8-O_3 concentrations in each region from 1981–2019 for bias-corrected and GEOS-Chem-simulated O_3. For the bias-corrected O_3, the averaged summertime MDA8-O_3 concentrations in BTHs, YRD, SCB and fall-time MDA8-O_3 concentrations in PRD are 137 ± 8 $\mu g\ m^{-3}$, 119 ± 10 $\mu g\ m^{-3}$, 113 ± 12 $\mu g\ m^{-3}$ and 98 ± 10 $\mu g\ m^{-3}$, with the increasing rate being 0.46 $\mu g\ m^{-3}\ yr^{-1}$, 0.73 $\mu g\ m^{-3}\ yr^{-1}$, 0.98 $\mu g\ m^{-3}\ yr^{-1}$ and 0.69 $\mu g\ m^{-3}\ yr^{-1}$ from 1981 to 2019, respectively (**Fig. S11**). For GEOS-Chem-simulated O_3, the averaged summertime MDA8-O_3 concentrations in BTHs, YRD, SCB and fall-time MDA8-O_3 concentrations in PRD are 141 ± 7 $\mu g\ m^{-3}$, 125 ± 11 $\mu g\ m^{3}$, 120 ± 14 $\mu g\ m^{-3}$ and 100 ± 12 $\mu g\ m^{-3}$, respectively. It shows that O_3 concentrations of the four regions have a consistent upward trend in the summer over the past decades, but there are regional differences in other seasons. Compared to BTHs and YRD, PRD and SCB have more distinctive O_3 increases in spring and fall. Among these four regions, the O_3 concentrations in BTHs have the biggest seasonal differences, but have the smallest seasonal differences in PRD.

The spatiotemporal patterns of O_3 in China have been proven to largely depend on both emissions and meteorology. The regional O_3 pollution is usually found to be triggered by specific circulation patterns as local meteorological factors are modulated by synoptic-scale circulation patterns. China has a large territory and is affected by different weather systems. The continental high-pressure systems, components of East Asian summer monsoon (EASM) and tropical cyclones, among others, are critical synoptic conditions leading to O_3 formation and transport in China (Wang et al., 2022b; Han et al., 2020). For instance, regional O_3 pollution in North China usually occurs under a typical weather pattern of an anomalous high-pressure system at 500 hPa (Gong and Liao, 2019), which creates favorable meteorological conditions for high O_3 levels with high temperature, low relative humidity, anomalous southerlies and divergence in the lower troposphere. As one of the most important components of EASM, the Western Pacific subtropical high (WPSH) strongly influences summertime precipitation and atmospheric conditions in East China. A strong WPSH can decrease O_3 levels over YRD as enhanced moisture is transported into YRD under prevailing southwesterly winds (Zhao and Wang, 2017). Located on the southern coast of China, PRD features a typical subtropical monsoon climate. There O_3 concentrations are usually the lowest in summer due to the prevailing southerlies with clean air from the ocean and the associated large rainfall, while the worst O_3 pollution usually happens in fall mainly due to the occasional northerly winds during the monsoonal transition, thereby importing precursors from the north, and stable and still relatively warm and sunny weather conditions before the winter starts. Downdrafts in the periphery circulation of a typhoon system can also strongly enhance surface O_3 before typhoon landing (Jiang et al., 2015; Lu et al., 2021; Li et al., 2022). On one the hand, the poor ventilation in the peripheral subsidence region of typhoons favors the accumulation of O_3 and its precursors. On the other hand, the deep subsidence can transport the O_3 in the upper troposphere and lower stratosphere to surface, causing aggravated O_3 pollution. Moreover, smaller-scale circulation patterns, such as land-sea and mountain-valley breezes, also influence O_3 in coastal regions (Ding et al., 2004; Zhou et al., 2013; Wang et al., 2018a).

When compared to the hybrid approach, GEOS-Chem generally has similar O_3 distribution and trends over each region, while overestimating O_3 concentrations (**Table S4**). GEOS-Chem particularly overestimates wintertime and fall-time O_3 concentrations in SCB, which are 10 ± 1 μg m^{-3} and 17 ± 3 μg m^{-3} higher than those of the hybrid approach, respectively. Previous studies reported such model overestimates and proposed a number of explanations involving precursor emissions, dry deposition, and vertical mixing in the planetary boundary layer (PBL) (Lin et al., 2008; Travis et al., 2016; Fiore et al., 2005). Both observational analyses and inter-model comparisons suggested that the summertime dry deposition of O_3 calculated by the Wesely scheme in GEOS-Chem could be underestimated, which has been invoked as a cause for model overestimates of O_3. The biased emissions in the model, as consistent with the biased-high tropospheric NO_x columns, result in overestimated O_3. Travis et al. (2016) showed that GEOS-Chem with reduced NO_x emissions provides an unbiased simulation of O_3 observations from the aircraft and reproduces the observed O_3 production efficiency in the boundary layer. Lin et al. (2008) suggested that the excessive PBL mixing can lead to the biased-high O_3 concentrations. The fully mixed O_3 throughout the PBL means that the higher O_3 concentrations in the upper PBL are brought down to the surface much more efficiently. Moreover, the excessive spatial averaging of emissions at coarser resolutions could also lead to systematic overestimation of regional O_3 production (Wild and Prather, 2006). In summary, with a higher prediction accuracy, the hybrid approach lends greater credence to using model simulations to extrapolate historical O_3 further back in time, which can furthermore provide us with more accurate estimates of O_3 impacts on crop production and human health.

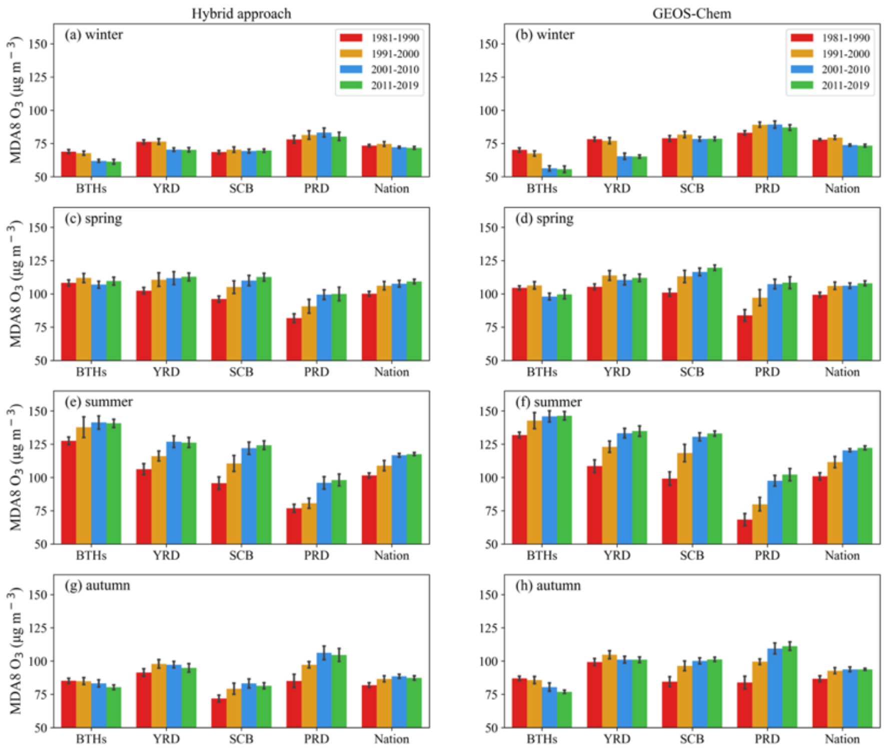

Figure 7. The seasonal mean MDA8-O_3 concentrations (μg m^{-3}) in different regions during 1981-2019. Bias-corrected MDA8-O_3 in: (a) winter; (c) spring; (e) summer; and (g) fall. GEOS-Chem MDA8-O_3 in: (b) winter; (d) spring; (f) summer; and (h) fall. The error bar represents the standard deviation.

3.5 Crop production losses attributable to O_3 pollution

Fig. 8 shows the relative yield losses (RYLs; RYL = 1 – RY, where RY is the relative yield defined as the ratio of the O_3-affected yield to the yield without O_3 exposure) calculated with GEOS-Chem and bias-corrected O_3 using AOT40-China metric. For a given crop, the RYLs show generally consistent spatial distribution across the metrics, with BTHs having the most serious crop yield losses due to high O_3 concentrations. Compared to the bias-corrected O_3, using GEOS-Chem-simulated O_3 generally leads to larger yield losses, especially over BTHs and SCB, reflecting overestimated O_3 concentrations by GEOS-Chem in cropland areas during the growing seasons (**Fig. S12**), primarily in spring and summer, which is consistent to the above analysis. GEOS-Chem-simulated O_3 leads to slightly underestimated wheat yield loss only over some parts of BTHs, mostly because the primary growing period of wheat there is in winter and spring, and GEOS-Chem has lower O_3 estimates than the hybrid approach during this period there (**Table S4**).

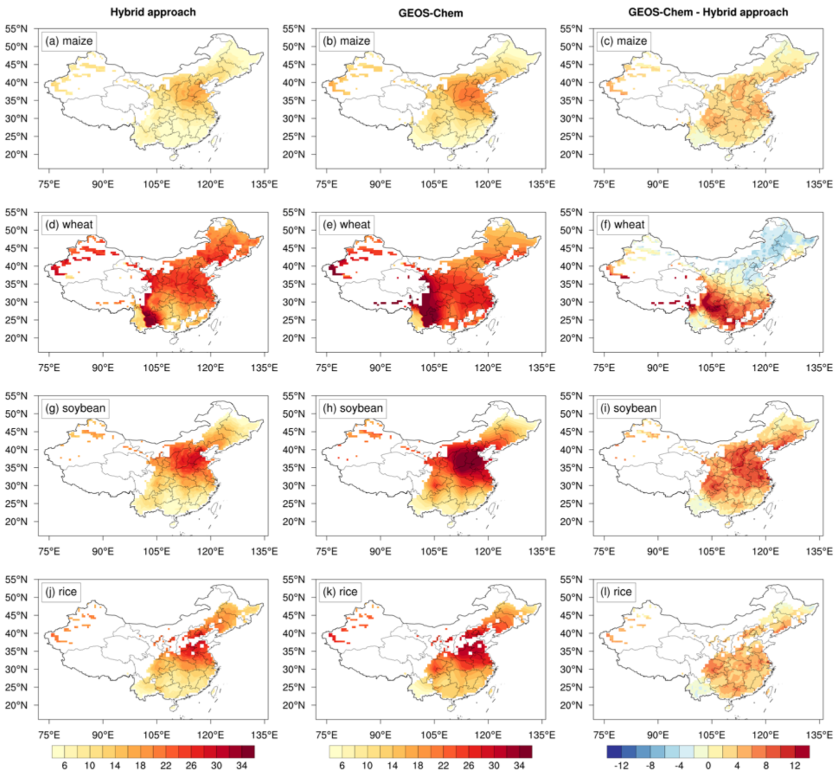

Figure 8. Estimated annual mean relative yield losses (RYLs, in %) of four staple crops from 1981–2019 using the AOT40-China metric. The estimated RYLs using bias-corrected O_3: (a) maize; (d) wheat; (g) soybean; and (j) rice. The estimated RYLs using GEOS-Chem-simulated O_3: (b) maize; (e) wheat; (h) soybean; and (k) rice. The differences in estimated RYLs between GEOS-Chem-simulated and bias-corrected O_3: (c) maize; (f) wheat; (i) soybean; and (l) rice. The GEOS-Chem-simulated O_3 were regridded to 0.5°×0.5° for comparison with bias-corrected O_3.

Fig. 9 shows the bar plots of the relative yield for each crop using AOT40-China exposure-yield response relationship. Crop yield losses are generally consistent with the O_3 trends as the exposure-yield relationships used here are essentially a set of linear functions. Most crops experience aggravated yield losses over the past four decades due to enhanced O_3 concentrations, except for wheat, which has the largest yield loss during the period 1991 to 2000. The reason could be that

BTHs have the highest O_3 concentrations in spring during the 1990s, which is the primary growing season for wheat (**Fig. S13**). Noticeable uncertainties of crop yield losses are found across metrics.

The average annual crop RYLs from 1981 to 2019 for wheat, rice, soybean and maize range from 1.1 to 13.4%, 2.7 to 13.4%, 6.3 to 24.8% and 0.8 to 7.4%, respectively. The differences in yield losses across crops reflect the dependence on crop-specific phenology and ecophysiology. The estimated annual RYLs using bias-corrected O_3 for wheat, rice, soybean and maize from 1981 to 2019 range from 17.5–25.5%, 10.7–19.1%, 7.3–17.9% and 7.1–12.7%, with a growth rate of 0.03% yr^{-1}, 0.04% yr^{-1}, 0.27% yr^{-1} and 0.13% yr^{-1}. Wheat is the most sensitive crop to the O_3 concentrations, whereas maize is the least sensitive. Using GEOS-Chem-simulated O_3, the estimated annual RYLs for wheat, rice, soybean and maize from 1981 to 2019 are 18.7–28.7%, 14.0–22.0%, 12.4–23.1%, and 7.9–13.2%, having a growth rate of 0.08% yr^{-1}, 0.14% yr^{-1}, 0.23% yr^{-1} and 0.11% yr^{-1}. There are noticeable differences in crop yield estimates using the bias-corrected and GEOS-Chem O_3, indicating again the importance of the bias-corrected high-resolution O_3 data in related crop issues.

In existing studies evaluating the O_3-induced crop losses in China, which also use exposure-yield relationship derived from the experiments conducted in Asia, Zhang et al. (2017) reported that the ambient O_3 concentrations in Northeast China cause substantial annual yield loss of soybean ranging from 23.4% to 30.2% during 2013 and 2014, depending on the O_3 metric used (including AOT40, W126, SUM06 and a flux-based metric). Feng et al. (2022), using AOT40, indicated that the annual average RYLs of wheat (33%), rice (23%) and maize (9%) from 2017 to 2019. Our correspondingly estimated RYLs for rice (18.0%) and maize (10.0%) are generally consistent to their results, while the RYLs for soybean (16.4%) and wheat (23.4%) are much lower than the estimates. Since we used the same exposure-yield response relationships in their studies, the discrepancies are primarily attributed to the differences in used metrics (only for soybean), O_3 fields and sensitivity of crop to the changes of O_3 concentrations (Mukherjee et al., 2021; Feng et al., 2022; Mills et al., 2018). In Zhang et al. (2017), the O_3 measurements are obtained from the experimental field (45°73′N, 126°61′E), and in Feng et al. (2022), the measured O_3 concentrations are from over 3,000 monitoring sites across East Asia. The results of comparison are consistent to the previous analysis of O_3 trends and variability from different sources, where the domain-average values of O_3 observations are larger than gridded O_3 from model simulations (**Section 3.2**) and thus lead to larger estimates of RYLs. On one hand, it indicates that O_3 fields should be considered as a great source of uncertainty when comparing the results of previous studies using source-varied O_3 fields. Moreover, different degrees of importance should be given for specific crops, for example, the changes in O_3 concentrations have a larger impact on wheat crop. On the other hand, it highlights again the necessity and importance of bias correction for model-simulated O_3 when O_3-inudec crop reduction.

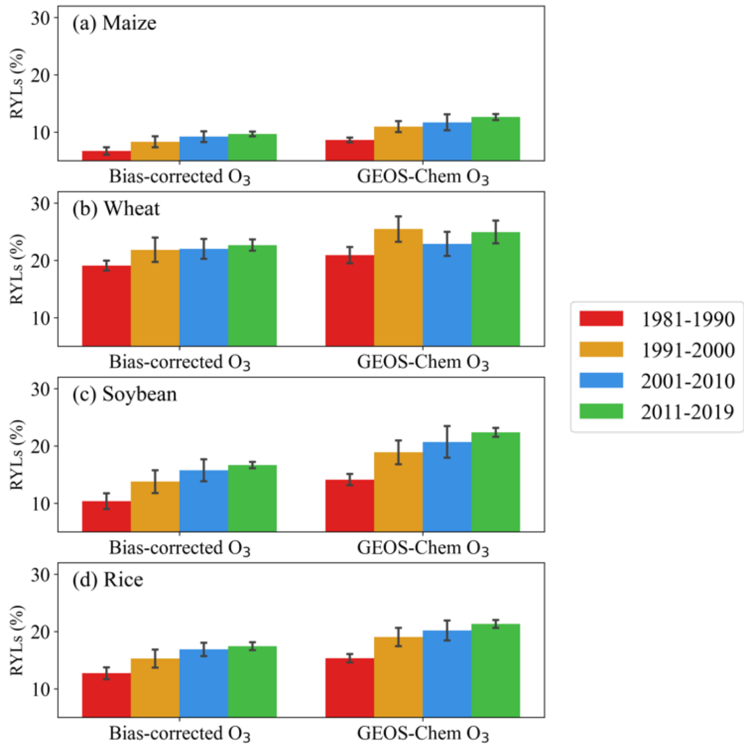

Figure 9. The estimated decadal mean relative yield losses (RYLs) of four staple crops using different metrics from 1981–2019. The estimated RYLs using bias-corrected O_3: (a) maize; (c) wheat; (e) soybean; and (g) rice. The estimated RYLs using GEOS-Chem-simulated O_3: (b) maize; (d) wheat; (f) soybean; and (h) rice. The error bar represents the standard deviation.

3.6 Health impacts attributable to O_3 pollution

The estimated annual all-cause premature deaths induced by O_3 increase from 55,876 in 1981 to 162,370 in 2019 with an increasing trend of +2,979 deaths yr^{-1}. The annual premature deaths related to respiratory and cardiovascular diseases are 34,155 and 40,323 in 1998, and 26,471 and 79,021 in 2019, having a rate of change of –546 and +1,773 deaths yr^{-1} during 1998–2019, respectively (**Fig. 10a**). Among three types of health outcomes, only respiratory diseases experienced a decreasing trend in premature mortality, and the premature mortality is constantly below 40,000. The decreasing trend of the respiration-related mortality primarily results from the decreased annual baseline mortality rate over the past decades (**Fig. S14**). As the total respiratory-related deaths decreased over the past decades, respiratory O_3 deaths are decreasing even under aggravated O_3 pollution. Based on GEOS-Chem-simulated O_3, the corresponding estimated change rate for all-cause disease is +3,516 deaths yr^{-1} from 50,384 in 1981 to 176,741 in 2019. Premature mortality induced by respiratory disease decreases from 37,822 in 1998 to 29,079 in 2019 with a change rate of –584 deaths yr^{-1}, while cardiovascular disease increases from 44,516 in 1998 to 85,980 in 2019 with a change rate of +1,977 deaths yr^{-1} (**Fig. S15**). The result shows that using GEOS-Chem-simulated O_3 generally gives higher estimates of mortality than using the bias-corrected data. **Fig. 10b** shows the provincial annual average premature mortality of different health endpoints. The five provinces with the highest all-cause mortality are Jiangsu [14,510 (95% CI: 9,022–19,935)], Shandong [12,684 (95% CI:4,258–20,990)], Henan [12,290 (95% CI: 4,125–20,343)], Guangdong [9,268 (95% CI: 7,224–11,416)] and Hebei [8,276 (95% CI: 2,776–13,706), which are generally consistent with previous studies for China (Zhang et al., 2021; Zhang et al., 2022a). Similar distribution can be found for respiratory and cardiovascular diseases but with a different ranking order. Generally, those provinces in densely populated areas (**Fig. 10c**) with higher O_3 concentrations, such as BTHs, YRD and PRD, have higher health burdens. In contrast, the northeastern and southern China (excluding Guangdong) suffer the least life losses induced by O_3 exposure (**Fig. S16**).

When compared with estimates from previous studies, our estimates of are generally quite consistent with that given by Maji and Namdeo (2021), which reported that the short-term all-cause, cardiovascular and respiratory premature mortalities attributed to ambient O_3 exposure were 156,000, 73,500 and 28,600 in 2019. Based on O_3 observations in 334 Chinese cities, Zhang et al. (2021) suggested that the national all-cause, respiratory, cardiovascular mortalities attributable to O_3 are 270,000 to 390,000, 49,000 to 63,000, and 150,000 to 220,000 across 2015–2018, which are much higher than most existing results. Since the methodological approaches are largely similar and we use the log-linear exposure-response function, we ascribe that the very high estimated mortalities are mainly due to concentration–response threshold X_0 assumed to be zero in their study. A lower X_0 means that O_3 can cause more adverse impacts on human health even at low concentrations, thus leading to higher mortalities.

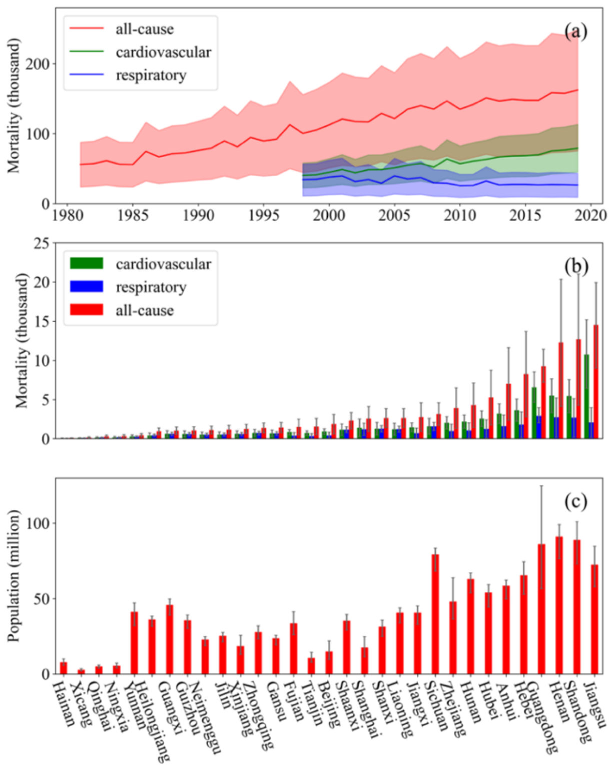

Figure 10. (a) Annual premature morality (thousand) for different diseases over the past decades; (b) annual mean province-based morality (thousand) attributed to different health endpoints; and (c) annual mean province-based population (million). The morality is calculated using the bias-corrected O_3.

4. Conclusions and discussion

In this study, to have a more accurate characterization of O_3 spatiotemporal distribution and trends as well as their impacts on agriculture and human health, we used a hybrid approach to generate bias-corrected O_3 data across China from 1981 to 2019. The hybrid approach helps improve O_3 predictions by taking advantage of a chemical transport model, a ML algorithm and increasing availability of high-resolution environmental and meteorological data. In the model training process, we found that utilizing a higher-resolution meteorological dataset, albeit one that is not the same as the default CTM input meteorology, has high potential to enhance the performance of the hybrid model in reproducing observed O_3 concentrations. The validation shows that the bias-corrected O_3 can achieve a higher prediction accuracy than GEOS-Chem-simulated O_3 alone when compared with historical in-situ measurements. Before being corrected, the GEOS-Chem-simulated O_3 concentrations tend to be overestimated and lead to higher crop yield losses and larger O_3-induced mortalities.

Noticeable differences in crop RYLs and mortality estimates highlight the advantages of using high-resolution O_3 data to improve our understanding of long-term O_3 impacts.

When examining the regional and national O_3 trends, we found that MDA8-O_3 concentrations have a perceptible increasing trend before 2000s, but fluctuate within a certain range with large interannual variabilities in more recent years. The large discrepancies in previous studies indicate that the regional and national O_3 trends in China still suffer with great uncertainties, particularly when different approaches are used to produce the O_3 estimates. However, these studies using source-varied O_3 fields consistently show the great interannual variabilities of O_3 concentrations. Some insights can be obtained from existing findings, which need to be carefully considered when examining O_3 trends and comparing them with existing results. First, given the large site differences, the calculation of observational O_3 trends is very sensitive to the subsets of data from networks. Thus, great uncertainty could still exist even using O_3 observations from the same source depending on the chosen subsets of data. Second, different formats of O_3 fields (e.g., site-based and gridded) could lead to large uncertainties of the O_3 trend estimates. A higher resolution of gridded O_3 estimates from CTMs and ML may reduce the differences between O_3 observational results. Third, the calculated O_3 trends are very sensitive to the chosen study period due to large interannual variability and seasonal differences. The changing meteorological conditions are the major factor causing the large interannual O_3 variations, and reductions in the emissions of NO_x, SO_2 and PM also have complex effects on ground-level O_3 concentrations (Wang et al., 2022b). Liu and Wang (2020a) suggested that the meteorological impacts on O_3 trends vary region by region and year by year and could be comparable with or even larger than the impacts of changes in anthropogenic emissions.

Our estimated RYLs for maize and rice and soybean in China are generally consistent to existing studies, while the RYLs for soybean and wheat are lower than their estimates mainly due to the differences in used metrics, O_3 fields and crop sensitivity to ambient O_3 concentrations. It suggests that plating O_3-resistant cultivars could be an effective approach to increase total crop production to meet the increasing food demands. In addition to the metrics and O_3 fields, uncertainties of estimated O_3-induced crop losses could be also from other sources (e.g., exposure-yield relationships). Though some other metrics (e.g., M7/M12 and W126) have also been used in some studies (Van Dingenen et al., 2009; Avnery et al., 2013; Wang et al., 2022c), there are not available exposure-yield relationships for all four major crops specific for China. The estimated RYLs for crops could be largely biased using metrics with exposure-yield relationships developed for U.S. or Europe (**Fig. S17**), as they are inadequate to represent Asian crop genotypes and environmental conditions. So, the region-specific exposure-yield relationships are highly recommended to be used in future study estimating the O_3-induced crop reduction, especially for the regional study.

In recent years, although existing studies have made efforts to quantify the O_3-related health impacts in China, only a few focused on the nationwide acute O_3 health burden assessment, particularly for assessment over multiple decades (Maji and Namdeo, 2021; Sahu et al., 2021; Zhang et al., 2021; Zhang et al., 2022a). There are some remaining issues to be addressed regarding O_3 health impacts. For instance, the existence of a “safe” threshold of O_3 levels still remains debated. A recent study reported that no consistent evidence was found for a threshold in the O_3-mortality concentration-response relationship in seven cities of Jiangsu Province, China during 2013–2014 (Chen et al., 2017; Maji and Namdeo, 2021). Given the importance of the threshold assumption in assessing health effects of air pollution, more studies are needed to determine a most likely threshold for O_3-mortality association in the future. Moreover, the multiple temporal O_3 metrics (e.g.,1-h maximum and daytime average O_3 concentrations) have also been proved to play an important role in the variability of estimated health effects, even though standard ratios are used to convert among multiple metrics (Anderson and Bell, 2010). In addition to the uncertainties from varying methodologies, interpretation of the O_3 epidemiological impact is also constrained by the variability in geographical, seasonal, and demographic characteristics (Yin et al., 2017b). Liu et al. (2013) suggested that associations between O_3 and mortality appeared to be more evident during the cool season than in the warm season, and stronger in the oldest age group and among those with less education. The effect modification by population susceptibility and the confounding effects of concomitant exposures (temperature, particulate matter, etc.) should be further considered in future works.

A major limitation of our study lies in the uncertain predictions in regions where monitoring data are scarce (e.g., the western half of China). The monitoring sites are sparsely distributed in those areas, which may fail to capture the accurate association between O_3 concentrations and various predictors there, especially considering that the ML algorithm has likely over-emphasized such relationships in the data-intensive eastern regions. Second, the land use data were prescribed in 2013 due to the limited availability of data, and this may neglect some major land use changes in China over the past decades. Though the land use data were found by the ML algorithm to contribute little to the overall model, more detailed land use data are expected to further increase model accuracy. In addition, though concentration-based metrics are easy to calculate and ensured to be scientifically sound in some experiments (Fuhrer et al., 1997; Mills et al., 2007), they do not consider the active responses of plant ecophysiology to ambient climatic and environmental changes and thus likely inadequate for examining yield losses in a future climate and atmospheric environment (Tai et al., 2021). So, flux-based metrics are recommended in future studies to better understand the long-term evolution of crop losses over China (Feng et al., 2012; Zhang et al., 2017; Tai et al., 2021; Pleijel et al., 2022), wherein more crop- and region-specific experiments and trials are needed to acquire appropriate metrics and exposure-yield response functions and calibrate the process-based crop model.

Despite these limitations, our study represents important progress in evaluating the long-term, multidecadal health burdens and agricultural losses resulting from O_3 pollution in China. Across the four major regions, BTHs experience the highest RYLs for major crops due to elevated O_3. On the other hand, the YRD and PRD regions have greater human health losses primarily due to their large population size. The results can provide important references for governments and agencies when making related national or regional policies to meet the imperative environment, health, and food security demands. To effectively address O_3 impacts, collaborative efforts can be made in multifaceted aspects: (1) to implement stricter regulations and specific emission control measures for major ozone precursors from industrial, vehicular and agricultural sources that account for region-specific chemical, meteorological and terrestrial conditions; (2) to encourage the adoption of more sustainable and adaptive agricultural practices that minimize O_3 exposure and its damage on crops (e.g., cultivating O_3-resistant crop varieties); (3) to improve short-range O_3 forecast capabilities of regional models, especially with the enhancement of artificial intelligence technology, which may enable better early warning systems to prepare the public and farmers for O_3 episodes; (4) to raise public awareness via promotional campaigns and educational programs to inform individuals, communities, and farmers about the risks associated with O_3. It is important for policymakers to consider these suggestions and act to effectively mitigate the negative O_3 impacts.

Data availability. Model output data used for analysis and plotting can be made available in nc format by contacting the corresponding author (Amos P. K. Tai at amostai@cuhk.edu.hk).

Competing interests. The authors declare that neither they nor their co-authors have any competing interests.

Author contributions. APKT designed the study and supervised the writing of the paper. JM conducted model simulation, analyzed results, and wrote the draft with the assistance of TGY and KTC. DHYY performed the GEOS-Chem simulations. ZZF assisted in the interpretation of the results. All authors contributed to the discussion and improvement of the paper.

Acknowledgements. This work was supported by the National Natural Science Foundation of China (NSFC)/Research Grants Council (RGC) Joint Research Scheme (reference #: N_CUHK440/20, 42061160479) awarded to A. P. K. Tai and Z. Feng.

References

Abdullah, S., Ismail, M., and Fong, S. Y.: Multiple Linear Regression (MLR) models for long term PM10 concentration forecasting during different monsoon seasons, Journal of Sustainability Science and Management, 12, 60-69, 2017.

Accadia, C., Mariani, S., Casaioli, M., Lavagnini, A., and Speranza, A.: Sensitivity of Precipitation Forecast Skill Scores to Bilinear Interpolation and a Simple Nearest-Neighbor Average Method on High-Resolution Verification Grids, Weather and Forecasting, 18, 918-932, https://doi.org/10.1175/1520-0434(2003)018<0918:SOPFSS>2.0.CO;2, 2003.

Anderson, G. B. and Bell, M. L.: Does one size fit all? The suitability of standard ozone exposure metric conversion ratios and implications for epidemiology, Journal of Exposure Science & Environmental Epidemiology, 20, 2-11, https://doi.org/10.1038/jes.2008.69, 2010.

Avnery, S., Mauzerall, D. L., and Fiore, A. M.: Increasing global agricultural production by reducing ozone damages via methane emission controls and ozone-resistant cultivar selection, Global Change Biology, 19, 1285-1299, https://doi.org/10.1111/gcb.12118, 2013.

Bey, I., Jacob, D. J., Yantosca, R. M., Logan, J. A., Field, B. D., Fiore, A. M., Li, Q., Liu, H. Y., Mickley, L. J., and Schultz, M. G.: Global modeling of tropospheric chemistry with assimilated meteorology: Model description and evaluation, Journal of Geophysical Research: Atmospheres, 106, 23073-23095, https://doi.org/10.1029/2001JD000807, 2001.

Bi, J., Knowland, K. E., Keller, C. A., and Liu, Y.: Combining Machine Learning and Numerical Simulation for High-Resolution PM2.5 Concentration Forecast, Environ Sci Technol, 56, 1544-1556, https://doi.org/10.1021/acs.est.1c05578, 2022.

Chen, K., Zhou, L., Chen, X., Bi, J., and Kinney, P. L.: Acute effect of ozone exposure on daily mortality in seven cities of Jiangsu Province, China: No clear evidence for threshold, Environmental Research, 155, 235-241, https://doi.org/10.1016/j.envres.2017.02.009, 2017.

Chen, T. and Guestrin, C.: XGBoost: A Scalable Tree Boosting System, Proceedings of the 22nd ACM SIGKDD International Conference on Knowledge Discovery and Data Mining, San Francisco, California, USA, https://doi.org/10.1145/2939672.2939785, 2016.

Clifton, O. E., Fiore, A. M., Massman, W. J., Baublitz, C. B., Coyle, M., Emberson, L., Fares, S., Farmer, D. K., Gentine, P., Gerosa, G., Guenther, A. B., Helmig, D., Lombardozzi, D. L., Munger, J. W., Patton, E. G., Pusede, S. E., Schwede, D. B., Silva, S. J., Sorgel, M., Steiner, A. L., and Tai, A. P. K.: Dry Deposition of Ozone over Land: Processes, Measurement, and Modeling, Rev Geophys, 58, https://doi.org/10.1029/2019RG000670, 2020.

Dang, R., Liao, H., and Fu, Y.: Quantifying the anthropogenic and meteorological influences on summertime surface ozone in China over 2012–2017, Science of The Total Environment, 754, 142394, https://doi.org/10.1016/j.scitotenv.2020.142394, 2021.

Dedoussi, I. C., Eastham, S. D., Monier, E., and Barrett, S. R. H.: Premature mortality related to United States cross-state air pollution, Nature, 578, 261-265, https://doi.org/10.1038/s41586-020-1983-8, 2020.

Di, Q., Rowland, S., Koutrakis, P., and Schwartz, J.: A hybrid model for spatially and temporally resolved ozone exposures in the continental United States, Journal of the Air & Waste Management Association, 67, 39-52, https://doi.org/10.1080/10962247.2016.1200159, 2017.

Ding, A., Wang, T., Zhao, M., Wang, T., and Li, Z.: Simulation of sea-land breezes and a discussion of their implications on the transport of air pollution during a multi-day ozone episode in the Pearl River Delta of China, Atmospheric Environment, 38, 6737-6750, https://doi.org/10.1016/j.atmosenv.2004.09.017, 2004.

Emberson, L. D., Büker, P., Ashmore, M. R., Mills, G., Jackson, L. S., Agrawal, M., Atikuzzaman, M. D., Cinderby, S., Engardt, M., Jamir, C., Kobayashi, K., Oanh, N. T. K., Quadir, Q. F., and Wahid, A.: A comparison of North American and Asian exposure–response data for ozone effects on crop yields, Atmospheric Environment, 43, 1945-1953, https://doi.org/10.1016/j.atmosenv.2009.01.005, 2009.

Feng, Z., Calatayud, V., Zhu, J., and Kobayashi, K.: Ozone exposure- and flux-based response relationships with photosynthesis of winter wheat under fully open air condition, Science of The Total Environment, 619-620, 1538-1544, https://doi.org/10.1016/j.scitotenv.2017.10.089, 2018.

Feng, Z., Tang, H., Uddling, J., Pleijel, H., Kobayashi, K., Zhu, J., Oue, H., and Guo, W.: A stomatal ozone flux–response relationship to assess ozone-induced yield loss of winter wheat in subtropical China, Environmental Pollution, 164, 16-23, https://doi.org/10.1016/j.envpol.2012.01.014, 2012.

Feng, Z., De Marco, A., Anav, A., Gualtieri, M., Sicard, P., Tian, H., Fornasier, F., Tao, F., Guo, A., and Paoletti, E.: Economic losses due to ozone impacts on human health, forest productivity and crop yield across China, Environ Int, 131, 104966, https://doi.org/10.1016/j.envint.2019.104966, 2019.

Feng, Z., Xu, Y., Kobayashi, K., Dai, L., Zhang, T., Agathokleous, E., Calatayud, V., Paoletti, E., Mukherjee, A., Agrawal, M., Park, R. J., Oak, Y. J., and Yue, X.: Ozone pollution threatens the production of major staple crops in East Asia, Nature Food, 3, 47-56, https://doi.org/10.1038/s43016-021-00422-6, 2022.

Fiore, A. M., Horowitz, L. W., Purves, D. W., Levy Ii, H., Evans, M. J., Wang, Y., Li, Q., and Yantosca, R. M.: Evaluating the contribution of changes in isoprene emissions to surface ozone trends over the eastern United States, Journal of Geophysical Research: Atmospheres, 110, https://doi.org/10.1029/2004JD005485, 2005.

Fu, Y. and Tai, A. P. K.: Impact of climate and land cover changes on tropospheric ozone air quality and public health in East Asia between 1980 and 2010, Atmos. Chem. Phys., 15, 10093-10106, https://doi.org/10.5194/acp-15-10093-2015, 2015.

Fuhrer, J., Skärby, L., and Ashmore, M. R.: Critical levels for ozone effects on vegetation in Europe, Environmental Pollution, 97, 91-106, https://doi.org/10.1016/S0269-7491(97)00067-5, 1997.

Fusco, A. C. and Logan, J. A.: Analysis of 1970–1995 trends in tropospheric ozone at Northern Hemisphere midlatitudes with the GEOS-CHEM model, Journal of Geophysical Research: Atmospheres, 108, https://doi.org/10.1029/2002JD002742, 2003.

Gong, C. and Liao, H.: A typical weather pattern for ozone pollution events in North China, Atmos. Chem. Phys., 19, 13725-13740, https://doi.org/10.5194/acp-19-13725-2019, 2019.

Gong, C., Yue, X., Liao, H., and Ma, Y.: A humidity-based exposure index representing ozone damage effects on vegetation, Environmental Research Letters, 16, https://doi.org/10.1088/1748-9326/abecbb, 2021.

Guenther, A. B., Jiang, X., Heald, C. L., Sakulyanontvittaya, T., Duhl, T., Emmons, L. K., and Wang, X.: The Model of Emissions of Gases and Aerosols from Nature version 2.1 (MEGAN2.1): an extended and updated framework for modeling biogenic emissions, Geosci. Model Dev., 5, 1471-1492, https://doi.org/10.5194/gmd-5-1471-2012, 2012.

Han, H., Liu, J., Shu, L., Wang, T., and Yuan, H.: Local and synoptic meteorological influences on daily variability in summertime surface ozone in eastern China, Atmos. Chem. Phys., 20, 203-222, https://doi.org/10.5194/acp-20-203-2020, 2020.

He, J., Wang, Y., Hao, J., Shen, L., and Wang, L.: Variations of surface O_3 in August at a rural site near Shanghai: influences from the West Pacific subtropical high and anthropogenic emissions, Environmental Science and Pollution Research, 19, 4016-4029, https://doi.org/10.1007/s11356-012-0970-5, 2012.

Hoesly, R. M., Smith, S. J., Feng, L., Klimont, Z., Janssens-Maenhout, G., Pitkanen, T., Seibert, J. J., Vu, L., Andres, R. J., Bolt, R. M., Bond, T. C., Dawidowski, L., Kholod, N., Kurokawa, J. I., Li, M., Liu, L., Lu, Z., Moura, M. C. P., O'Rourke, P. R., and Zhang, Q.: Historical (1750–2014) anthropogenic emissions of reactive gases and aerosols from the Community Emissions Data System (CEDS), Geosci. Model Dev., 11, 369-408, https://doi.org/10.5194/gmd-11-369-2018, 2018.

Hu, X., Belle, J. H., Meng, X., Wildani, A., Waller, L. A., Strickland, M. J., and Liu, Y.: Estimating PM2.5 Concentrations in the Conterminous United States Using the Random Forest Approach, Environ Sci Technol, 51, 6936-6944, https://doi.org/10.1021/acs.est.7b01210, 2017.

Irrgang, C., Boers, N., Sonnewald, M., Barnes, E. A., Kadow, C., Staneva, J., and Saynisch-Wagner, J.: Towards neural

Earth system modelling by integrating artificial intelligence in Earth system science, Nature Machine Intelligence, 3, 667-674, https://doi.org/10.1038/s42256-021-00374-3, 2021.

Ivatt, P. D. and Evans, M. J.: Improving the prediction of an atmospheric chemistry transport model using gradient-boosted regression trees, Atmos. Chem. Phys., 20, 8063-8082, https://doi.org/10.5194/acp-20-8063-2020, 2020.

Jacob, D. J. and Winner, D. A.: Effect of climate change on air quality, Atmospheric Environment, 43, 51-63, https://doi.org/10.1016/j.atmosenv.2008.09.051, 2009.

Jiang, Y. C., Zhao, T. L., Liu, J., Xu, X. D., Tan, C. H., Cheng, X. H., Bi, X. Y., Gan, J. B., You, J. F., and Zhao, S. Z.: Why does surface ozone peak before a typhoon landing in southeast China?, Atmos. Chem. Phys., 15, 13331-13338, https://doi.org/10.5194/acp-15-13331-2015, 2015.

Kawase, H., Nagashima, T., Sudo, K., and Nozawa, T.: Future changes in tropospheric ozone under Representative Concentration Pathways (RCPs), Geophysical Research Letters, 38, https://doi.org/10.1029/2010GL046402, 2011.

Lelieveld, J., Evans, J. S., Fnais, M., Giannadaki, D., and Pozzer, A.: The contribution of outdoor air pollution sources to premature mortality on a global scale, Nature, 525, 367-371, https://doi.org/10.1038/nature15371, 2015.

Li, K., Jacob, D. J., Shen, L., Lu, X., De Smedt, I., and Liao, H.: Increases in surface ozone pollution in China from 2013 to 2019: anthropogenic and meteorological influences, Atmos. Chem. Phys., 20, 11423-11433, https://doi.org/10.5194/acp-20-11423-2020, 2020.

Li, Y., Zhao, X., Deng, X., and Gao, J.: The impact of peripheral circulation characteristics of typhoon on sustained ozone episodes over the Pearl River Delta region, China, Atmos. Chem. Phys., 22, 3861-3873, https://doi.org/10.5194/acp-22-3861-2022, 2022.

Lin, J. T., Youn, D., Liang, X. Z., and Wuebbles, D. J.: Global model simulation of summertime U.S. ozone diurnal cycle and its sensitivity to PBL mixing, spatial resolution, and emissions, Atmospheric Environment, 42, 8470-8483, https://doi.org/10.1016/j.atmosenv.2008.08.012, 2008.

Liu, H., Liu, S., Xue, B., Lv, Z., Meng, Z., Yang, X., Xue, T., Yu, Q., and He, K.: Ground-level ozone pollution and its health impacts in China, Atmospheric Environment, 173, 223-230, https://doi.org/10.1016/j.atmosenv.2017.11.014, 2018.

Liu, J., Wang, L., Li, M., Liao, Z., Sun, Y., Song, T., Gao, W., Wang, Y., Li, Y., Ji, D., Hu, B., Kerminen, V. M., Wang, Y., and Kulmala, M.: Quantifying the impact of synoptic circulation patterns on ozone variability in northern China from April to October 2013–2017, Atmos. Chem. Phys., 19, 14477-14492, https://doi.org/10.5194/acp-19-14477-2019, 2019.

Liu, R., Ma, Z., Liu, Y., Shao, Y., Zhao, W., and Bi, J.: Spatiotemporal distributions of surface ozone levels in China from 2005 to 2017: A machine learning approach, Environ Int, 142, 105823, https://doi.org/10.1016/j.envint.2020.105823, 2020.

Liu, T., Li, T. T., Zhang, Y. H., Xu, Y. J., Lao, X. Q., Rutherford, S., Chu, C., Luo, Y., Zhu, Q., Xu, X. J., Xie, H. Y., Liu, Z. R., and Ma, W. J.: The short-term effect of ambient ozone on mortality is modified by temperature in Guangzhou, China, Atmospheric Environment, 76, 59-67, https://doi.org/10.1016/j.atmosenv.2012.07.011, 2013.

Liu, Y. and Wang, T.: Worsening urban ozone pollution in China from 2013 to 2017 – Part 1: The complex and varying roles of meteorology, Atmos. Chem. Phys., 20, 6305-6321, https://doi.org/10.5194/acp-20-6305-2020, 2020a.

Liu, Y. and Wang, T.: Worsening urban ozone pollution in China from 2013 to 2017 – Part 2: The effects of emission changes and implications for multi-pollutant control, Atmos. Chem. Phys., 20, 6323-6337, https://doi.org/10.5194/acp-20-6323-2020, 2020b.

Lu, C., Mao, J., Wang, L., Guan, Z., Zhao, G., and Li, M.: An unusual high ozone event over the North and Northeast China during the record-breaking summer in 2018, J Environ Sci (China), 104, 264-276, https://doi.org/10.1016/j.jes.2020.11.030, 2021.

Lu, X., Hong, J., Zhang, L., Cooper, O. R., Schultz, M. G., Xu, X., Wang, T., Gao, M., Zhao, Y., and Zhang, Y.: Severe

Surface Ozone Pollution in China: A Global Perspective, Environmental Science & Technology Letters, 5, 487-494, https://doi.org/10.1021/acs.estlett.8b00366, 2018.

Lu, X., Zhang, L., Chen, Y., Zhou, M., Zheng, B., Li, K., Liu, Y., Lin, J., Fu, T.-M., and Zhang, Q.: Exploring 2016–2017 surface ozone pollution over China: source contributions and meteorological influences, Atmos. Chem. Phys., 19, 8339-8361, https://doi.org/10.5194/acp-19-8339-2019, 2019.

Ma, R., Ban, J., Wang, Q., Zhang, Y., Yang, Y., He, M. Z., Li, S., Shi, W., and Li, T.: Random forest model based fine scale spatiotemporal O_3 trends in the Beijing-Tianjin-Hebei region in China, 2010 to 2017, Environmental Pollution, 276, 116635, https://doi.org/10.1016/j.envpol.2021.116635, 2021.

Madaniyazi, L., Nagashima, T., Guo, Y., Pan, X., and Tong, S.: Projecting ozone-related mortality in East China, Environment International, 92-93, 165-172, https://doi.org/10.1016/j.envint.2016.03.040, 2016.

Maji, K. J. and Namdeo, A.: Continuous increases of surface ozone and associated premature mortality growth in China during 2015–2019, Environmental Pollution, 269, 116183, https://doi.org/10.1016/j.envpol.2020.116183, 2021.

Mao, J., Wang, L., Lu, C., Liu, J., Li, M., Tang, G., Ji, D., Zhang, N., and Wang, Y.: Meteorological mechanism for a large-scale persistent severe ozone pollution event over eastern China in 2017, J Environ Sci (China), 92, 187-199, https://doi.org/10.1016/j.jes.2020.02.019, 2020.

Meng, X., Wang, W., Shi, S., Zhu, S., Wang, P., Chen, R., Xiao, Q., Xue, T., Geng, G., Zhang, Q., Kan, H., and Zhang, H.: Evaluating the spatiotemporal ozone characteristics with high-resolution predictions in mainland China, 2013–2019, Environmental Pollution, 299, 118865, https://doi.org/10.1016/j.envpol.2022.118865, 2022.

Mills, G., Buse, A., Gimeno, B., Bermejo, V., Holland, M., Emberson, L., and Pleijel, H.: A synthesis of AOT40-based response functions and critical levels of ozone for agricultural and horticultural crops, Atmospheric Environment, 41, 2630-2643, https://doi.org/10.1016/j.atmosenv.2006.11.016, 2007.

Mills, G., Sharps, K., Simpson, D., Pleijel, H., Frei, M., Burkey, K., Emberson, L., Uddling, J., Broberg, M., Feng, Z., Kobayashi, K., and Agrawal, M.: Closing the global ozone yield gap: Quantification and cobenefits for multistress tolerance, Global Change Biology, 24, 4869-4893, https://doi.org/10.1111/gcb.14381, 2018.

Monfreda, C., Ramankutty, N., and Foley, J. A.: Farming the planet: 2. Geographic distribution of crop areas, yields, physiological types, and net primary production in the year 2000, Global Biogeochemical Cycles, 22, https://doi.org/10.1029/2007GB002947, 2008.

Moustris, K. P., Nastos, P. T., Larissi, I. K., and Paliatsos, A. G.: Application of Multiple Linear Regression Models and Artificial Neural Networks on the Surface Ozone Forecast in the Greater Athens Area, Greece, Advances in Meteorology, 2012, 894714, https://doi.org/10.1155/2012/894714, 2012.

Mukherjee, A., Yadav, D. S., Agrawal, S. B., and Agrawal, M.: Ozone a persistent challenge to food security in India: Current status and policy implications, Current Opinion in Environmental Science & Health, 19, 100220, https://doi.org/10.1016/j.coesh.2020.10.008, 2021.

Pleijel, H., Danielsson, H., and Broberg, M. C.: Benefits of the Phytotoxic Ozone Dose (POD) index in dose-response functions for wheat yield loss, Atmospheric Environment, 268, 118797, https://doi.org/10.1016/j.atmosenv.2021.118797, 2022.

Sacks, W. J., Deryng, D., Foley, J. A., and Ramankutty, N.: Crop planting dates: an analysis of global patterns, Global Ecology and Biogeography, 19, 607-620, https://doi.org/10.1111/j.1466-8238.2010.00551.x, 2010.

Sahu, S. K., Liu, S., Liu, S., Ding, D., and Xing, J.: Ozone pollution in China: Background and transboundary contributions to ozone concentration & related health effects across the country, Sci Total Environ, 761, 144131, https://doi.org/10.1016/j.scitotenv.2020.144131, 2021.

Shang, Y., Sun, Z., Cao, J., Wang, X., Zhong, L., Bi, X., Li, H., Liu, W., Zhu, T., and Huang, W.: Systematic review of Chinese studies of short-term exposure to air pollution and daily mortality, Environment International, 54, 100-111, https://doi.org/10.1016/j.envint.2013.01.010, 2013.

Sindelarova, K., Granier, C., Bouarar, I., Guenther, A., Tilmes, S., Stavrakou, T., Müller, J. F., Kuhn, U., Stefani, P., and Knorr, W.: Global data set of biogenic VOC emissions calculated by the MEGAN model over the last 30 years, Atmos. Chem. Phys., 14, 9317-9341, https://doi.org/10.5194/acp-14-9317-2014, 2014.

Tai, A. P. K., Mickley, L. J., Heald, C. L., and Wu, S.: Effect of CO_2 inhibition on biogenic isoprene emission: Implications for air quality under 2000 to 2050 changes in climate, vegetation, and land use, Geophysical Research Letters, 40, 3479-3483, https://doi.org/10.1002/grl.50650, 2013.

Tai, A. P. K., Sadiq, M., Pang, J. Y. S., Yung, D. H. Y., and Feng, Z.: Impacts of Surface Ozone Pollution on Global Crop Yields: Comparing Different Ozone Exposure Metrics and Incorporating Co-effects of CO_2, Frontiers in Sustainable Food Systems, 5, https://doi.org/10.3389/fsufs.2021.534616, 2021.

Thongthammachart, T., Araki, S., Shimadera, H., Eto, S., Matsuo, T., and Kondo, A.: An integrated model combining random forests and WRF/CMAQ model for high accuracy spatiotemporal PM2.5 predictions in the Kansai region of Japan, Atmospheric Environment, 262, https://doi.org/10.1016/j.atmosenv.2021.118620, 2021.

Travis, K. R., Jacob, D. J., Fisher, J. A., Kim, P. S., Marais, E. A., Zhu, L., Yu, K., Miller, C. C., Yantosca, R. M., Sulprizio, M. P., Thompson, A. M., Wennberg, P. O., Crounse, J. D., St. Clair, J. M., Cohen, R. C., Laughner, J. L., Dibb, J. E., Hall, S. R., Ullmann, K., Wolfe, G. M., Pollack, I. B., Peischl, J., Neuman, J. A., and Zhou, X.: Why do models overestimate surface ozone in the Southeast United States?, Atmos. Chem. Phys., 16, 13561-13577, https://doi.org/10.5194/acp-16-13561-2016, 2016.

van der Werf, G. R., Randerson, J. T., Giglio, L., van Leeuwen, T. T., Chen, Y., Rogers, B. M., Mu, M., van Marle, M. J. E., Morton, D. C., Collatz, G. J., Yokelson, R. J., and Kasibhatla, P. S.: Global fire emissions estimates during 1997–2016, Earth Syst. Sci. Data, 9, 697-720, https://doi.org/10.5194/essd-9-697-2017, 2017.

Van Dingenen, R., Dentener, F. J., Raes, F., Krol, M. C., Emberson, L., and Cofala, J.: The global impact of ozone on agricultural crop yields under current and future air quality legislation, Atmospheric Environment, 43, 604-618, https://doi.org/10.1016/j.atmosenv.2008.10.033, 2009.

Wang, H., Lyu, X., Guo, H., Wang, Y., Zou, S., Ling, Z., Wang, X., Jiang, F., Zeren, Y., Pan, W., Huang, X., and Shen, J.: Ozone pollution around a coastal region of South China Sea: interaction between marine and continental air, Atmos. Chem. Phys., 18, 4277-4295, https://doi.org/10.5194/acp-18-4277-2018, 2018a.

Wang, H., Lu, X., Jacob, D. J., Cooper, O. R., Chang, K. L., Li, K., Gao, M., Liu, Y., Sheng, B., Wu, K., Wu, T., Zhang, J., Sauvage, B., Nédélec, P., Blot, R., and Fan, S.: Global tropospheric ozone trends, attributions, and radiative impacts in 1995–2017: an integrated analysis using aircraft (IAGOS) observations, ozonesonde, and multi-decadal chemical model simulations, Atmos. Chem. Phys., 22, 13753-13782, https://doi.org/10.5194/acp-22-13753-2022, 2022a.

Wang, L., Tai, A. P. K., Tam, C.-Y., Sadiq, M., Wang, P., and Cheung, K. K. W.: Impacts of future land use and land cover change on mid-21st-century surface ozone air quality: distinguishing between the biogeophysical and biogeochemical effects, Atmos. Chem. Phys., 20, 11349-11369, https://doi.org/10.5194/acp-20-11349-2020, 2020.

Wang, L., Wang, S., Zhou, Y., Liu, W., Hou, Y., Zhu, J., and Wang, F.: Mapping population density in China between 1990 and 2010 using remote sensing, Remote Sensing of Environment, 210, 269-281, https://doi.org/10.1016/j.rse.2018.03.007, 2018b.

Wang, T., Xue, L., Feng, Z., Dai, J., Zhang, Y., and Tan, Y.: Ground-level ozone pollution in China: a synthesis of recent findings on influencing factors and impacts, Environmental Research Letters, 17, 063003, https://doi.org/10.1088/1748-9326/ac69fe, 2022b.

Wang, X., Gong, G., Li, N., and Qiu, S.: Detection Analysis of Epileptic EEG Using a Novel Random Forest Model Combined With Grid Search Optimization, Frontiers in Human Neuroscience, 13, https://doi.org/10.3389/fnhum.2019.00052, 2019.

Wang, Y., Zhang, Y., Hao, J., and Luo, M.: Seasonal and spatial variability of surface ozone over China: contributions from background and domestic pollution, Atmos. Chem. Phys., 11, 3511-3525, https://doi.org/10.5194/acp-11-3511-2011,

2011.
Wang, Y., Wild, O., Ashworth, K., Chen, X., Wu, Q., Qi, Y., and Wang, Z.: Reductions in crop yields across China from elevated ozone, Environmental Pollution, 292, 118218, https://doi.org/10.1016/j.envpol.2021.118218, 2022c.
Wei, J., Li, Z., Li, K., Dickerson, R. R., Pinker, R. T., Wang, J., Liu, X., Sun, L., Xue, W., and Cribb, M.: Full-coverage mapping and spatiotemporal variations of ground-level ozone (O_3) pollution from 2013 to 2020 across China, Remote Sensing of Environment, 270, 112775, https://doi.org/10.1016/j.rse.2021.112775, 2022.
Wesely, M. L.: Parameterization of surface resistances to gaseous dry deposition in regional-scale numerical models, Atmospheric Environment (1967), 23, 1293-1304, https://doi.org/10.1016/0004-6981(89)90153-4, 1989.
Wild, O. and Prather, M. J.: Global tropospheric ozone modeling: Quantifying errors due to grid resolution, Journal of Geophysical Research: Atmospheres, 111, https://doi.org/10.1029/2005JD006605, 2006.
Xiao, Q., Chang, H. H., Geng, G., and Liu, Y.: An Ensemble Machine-Learning Model To Predict Historical PM2.5 Concentrations in China from Satellite Data, Environmental Science & Technology, 52, 13260-13269, https://doi.org/10.1021/acs.est.8b02917, 2018.
Yang, L., Luo, H., Yuan, Z., Zheng, J., Huang, Z., Li, C., Lin, X., Louie, P. K. K., Chen, D., and Bian, Y.: Quantitative impacts of meteorology and precursor emission changes on the long-term trend of ambient ozone over the Pearl River Delta, China, and implications for ozone control strategy, Atmos. Chem. Phys., 19, 12901-12916, https://doi.org/10.5194/acp-19-12901-2019, 2019.
Yin, H., Pizzol, M., and Xu, L.: External costs of PM2.5 pollution in Beijing, China: Uncertainty analysis of multiple health impacts and costs, Environmental Pollution, 226, 356-369, https://doi.org/10.1016/j.envpol.2017.02.029, 2017a.
Yin, P., Chen, R., Wang, L., Meng, X., Liu, C., Niu, Y., Lin, Z., Liu, Y., Liu, J., Qi, J., You, J., Zhou, M., and Kan, H.: Ambient Ozone Pollution and Daily Mortality: A Nationwide Study in 272 Chinese Cities, Environ Health Perspect, 125, 117006, https://doi.org/10.1289/EHP1849, 2017b.
Yin, Z. and Ma, X.: Meteorological conditions contributed to changes in dominant patterns of summer ozone pollution in Eastern China, Environmental Research Letters, 15, https://doi.org/10.1088/1748-9326/abc915, 2020.
Zhan, Y., Luo, Y., Deng, X., Chen, H., Grieneisen, M. L., Shen, X., Zhu, L., and Zhang, M.: Spatiotemporal prediction of continuous daily PM2.5 concentrations across China using a spatially explicit machine learning algorithm, Atmospheric Environment, 155, 129-139, https://doi.org/10.1016/j.atmosenv.2017.02.023, 2017.
Zhang, W., Feng, Z., Wang, X., Liu, X., and Hu, E.: Quantification of ozone exposure- and stomatal uptake-yield response relationships for soybean in Northeast China, Science of The Total Environment, 599-600, 710-720, https://doi.org/10.1016/j.scitotenv.2017.04.231, 2017.
Zhang, X., Osei, F., Stein, A., Cheng, C., and Maji, K. J.: Temporal and spatial evolution of short-term exposure to ozone pollution: Its health impacts in China based on a meta-analysis, Journal of Cleaner Production, 373, 133938, https://doi.org/10.1016/j.jclepro.2022.133938, 2022a.
Zhang, X., Yan, B., Zhou, Y., Osei, F., Li, Y., Zhao, H., Cheng, C., and Stein, A.: Short-term health impacts related to ozone in China before and after implementation of policy measures: A systematic review and meta-analysis, Science of The Total Environment, 847, 157588, https://doi.org/10.1016/j.scitotenv.2022.157588, 2022b.
Zhang, Y., Wang, Y., Gao, M., Ma, Q., Zhao, J., Zhang, R., Wang, Q., and Huang, L.: A Predictive Data Feature Exploration-Based Air Quality Prediction Approach, IEEE Access, 7, 30732-30743, https://doi.org/10.1109/ACCESS.2019.2897754, 2019.
Zhang, Z., Yao, M., Wu, W., Zhao, X., and Zhang, J.: Spatiotemporal assessment of health burden and economic losses attributable to short-term exposure to ground-level ozone during 2015-2018 in China, BMC Public Health, 21, 1069, https://doi.org/10.1186/s12889-021-10751-7, 2021.
Zhao, Z. and Wang, Y.: Influence of the West Pacific subtropical high on surface ozone daily variability in summertime over eastern China, Atmospheric Environment, 170, 197-204, https://doi.org/10.1016/j.atmosenv.2017.09.024, 2017.

Zhou, D., Ding, A., Mao, H., Fu, C., Wang, T., Chan, L. Y., Ding, K., Zhang, Y., Liu, J., Lu, A., and Hao, N.: Impacts of the East Asian monsoon on lower tropospheric ozone over coastal South China, Environmental Research Letters, 8, 044011, https://doi.org/10.1088/1748-9326/8/4/044011, 2013.